A STRIPAK complex mediates axonal transport of autophagosomes and dense core vesicles through PP2A regulation

Amanda L. Neisch, Thomas P. Neufeld, and Thomas S. Hays

Department of Genetics, Cell Biology, and Development, University of Minnesota, Minneapolis, MN 55455

Autophagy plays an essential role in the cellular homeostasis of neurons, facilitating the clearance of cellular debris. This clearance process is orchestrated through the assembly, transport, and fusion of autophagosomes with lysosomes for degradation. The motor protein dynein drives autophagosome motility from distal sites of assembly to sites of lysosomal fusion. In this study, we identify the scaffold protein CKA (connector of kinase to AP-1) as essential for autophagosome transport in neurons. Together with other core components of the striatin-interacting phosphatase and kinase (STRIPAK) complex, we show that CKA associates with dynein and directly binds Atg8a, an autophagosomal protein. CKA is a regulatory subunit of PP2A, a component of the STRIPAK complex. We propose that the STRIPAK complex modulates dynein activity. Consistent with this hypothesis, we provide evidence that CKA facilitates axonal transport of dense core vesicles and autophagosomes in a PP2A-dependent fashion. In addition, CKA-deficient flies exhibit PP2A-dependent motor coordination defects. CKA function within the STRIPAK complex is crucial to prevent transport defects that may contribute to neurodegeneration.

Introduction

As postmitotic cells with an extended morphology and life span, neurons are especially sensitive to cellular insults that result in the accumulation of damaged proteins and organelles. Macroautophagy, herein referred to as autophagy, is an essential cellular process that functions to promote cellular homeostasis and is critical in neurons for clearing cellular debris and maintaining synaptic function and cell health. Indeed, defects in autophagy have been linked to several neurodegenerative disorders, including Alzheimer's disease (Nixon et al., 2005) and amyotropic lateral sclerosis (Ikenaka et al., 2013).

Autophagy gives rise to the formation of a vesicular double-membrane organelle, termed the autophagosome, that encapsulates a portion of the cytoplasm along with damaged proteins and organelles (Meléndez and Neufeld, 2008; Mizushima et al., 2010). The eventual clearance of autophagosomes and their engulfed contents is mediated by cytoplasmic dynein, the retrograde molecular motor that delivers autophagosomes to their sites of fusion with lysosomes (Ravikumar et al., 2005; Kimura et al., 2008; Maday et al., 2012; Xu et al., 2013). Fusion of the autophagosome with the lysosome forms an acidified hybrid organelle, the autolysosome, in which degradation of the engulfed contents of the autophagosome occurs.

Autophagosomes accumulate in the neurons of neurodegenerative disease patients (Nixon et al., 2005; Ikenaka et al., 2013), suggesting that a defect in proper autophagosome clearance may contribute to disease progression. Indeed, in *Drosophila melanogaster*, when autophagosome–lysosome fusion is defective, autophagosomes accumulate in neurons, and these animals have locomotor defects and decreased life spans (Takáts et al., 2013). Collectively, these results suggest that autophagosome clearance is crucial for neuronal function. However, the mechanisms that regulate autophagy in neurons are not well understood. In particular, given the unique morphology of neurons, there is considerable interest in identifying the regulatory machineries involved in the targeting, attachment, and cytoskeletal transport of autophagosomes.

Scaffolding and adaptor proteins have emerged as key regulators of motor-driven organelle transport along microtubules, often acting to physically link motors and their cargoes (Schlager and Hoogenraad, 2009; Fu and Holzbaur, 2014). Scaffolding proteins can provide an additional level of regulation through their association with posttranslational protein modifiers, such as kinases and phosphatases (Yasuda et al., 1999; Kelkar et al., 2000; Willoughby et al., 2003; Horiuchi et al., 2007). The tethering of kinase and phosphatase activities to scaffold complexes provides a mechanism by which the motors,

Correspondence to Thomas S. Hays: haysx001@umn.edu

Abbreviations used: ANF, atrial natriuretic factor; CKA, connector of kinase to AP-1; DCV, dense core vesicle; LIR, LC3-interacting region; Mts, microtubule star; NMJ, neuromuscular junction; PE, phosphatidylethanolamine; Strip, striatin-interacting protein; STRIPAK, striatin-interacting phosphatase and kinase; VNC, ventral nerve cord.

The Rockefeller University Press $30.00
J. Cell Biol. Vol. 216 No. 2 441–461
https://doi.org/10.1083/jcb.201606082

cargo attachments, and directed transport can be locally regulated. Using the strength of *Drosophila* genetics, we identify in this study a scaffolding protein, connector of kinase to AP-1 (CKA), as a new regulator of axonal transport.

CKA is homologous to the striatin family of proteins in mammals (Chen et al., 2002). CKA and striatin proteins are regulatory subunits of the serine/threonine phosphatase protein phosphatase 2A (PP2A). In addition, they are scaffolding proteins for the striatin-interacting phosphatase and kinase (STRIPAK) complex (Goudreault et al., 2009; Ribeiro et al., 2010). The STRIPAK complex is a large molecular complex that is highly conserved from fungi to humans and contains PP2A and typically a sterile-20 kinase. PP2A is a holoenzyme consisting of a catalytic subunit, a structural subunit, and a regulatory subunit. Although the structural subunit provides the linkage between the catalytic and regulatory subunits, the regulatory subunit controls the subcellular localization or substrate specificity of the phosphatase activity. The core components of the mammalian STRIPAK complex are striatin family proteins (PP2A regulatory subunits), a PP2A catalytic subunit, a PP2A structural subunit, Mps one binder kinase activator-like 3 (Mob3), cerebral cavernous malformation 3 (Ccm3), striatin-interacting proteins 1 and 2 (STRIP1/STRIP2), and the germinal center kinase III (GckIII) subfamily of kinases MST4, STK24, and STK25 (Goudreault et al., 2009; Kean et al., 2011). The STRIPAK complex is conserved in *Drosophila*, and its core components consist of CKA (the sole striatin protein), microtubule star (Mts; the sole PP2A catalytic subunit), PP2A at 29B (Pp2A-29B; the sole PP2A structural subunit), Mob4 (orthologue of Mob3), Ccm3, Strip (orthologue of STRIP1), and GckIII (Ribeiro et al., 2010). In addition to the core components, the STRIPAK complex contains a less well-characterized set of STRIPAK-associated proteins, some of which appear to be mutually exclusive (Goudreault et al., 2009; Ribeiro et al., 2010; Hyodo et al., 2012; Couzens et al., 2013). Reflective of the variation in protein compositions, striatins and related STRIPAK complexes have been connected to multiple clinical conditions, including autism, cerebral malformation, cardiac disease, cancer, and diabetes (Hwang and Pallas, 2014).

In the present study, we identify and characterize the role of CKA and the STRIPAK complex in axonal transport. Similar to dynein depletion, reducing CKA or STRIPAK components disrupts autophagosome transport in motoneurons. We find that CKA is present in a complex with dynein, and binds directly to the autophagosomal membrane protein Atg8a. We show that the STRIPAK components CKA, Mob4, and Strip also participate in the transport of dense core vesicles (DCVs), but not mitochondria. This transport is dependent on the association of the phosphatase PP2A with CKA. Our findings demonstrate that a STRIPAK complex functions to regulate the transport of a subset of organelles important for both protein/organelle turnover and neuronal signaling, and that CKA's function within the nervous system is essential for locomotion and viability.

Results

Dynein depletion disrupts autophagosome distribution in neurons

To study the transport of autophagosomes in an intact nervous system, we used *Drosophila* larval motoneurons with established and stereotyped synaptic connections (Fig. 1 A). We monitored the distribution of autophagosomes using the autophagy-related protein, Atg8a. Atg8a, homologous to LC3 in mammals, is a cytoplasmic protein that upon autophagy induction is covalently linked to phosphatidylethanolamine (PE) on autophagosomal membranes (Mauvezin et al., 2014; Shibutani and Yoshimori, 2014). To specifically label autophagosomes, we expressed a dual-tagged mCherry (mCh)-GFP-Atg8a protein (Takáts et al., 2013) in motoneurons using the driver *Ok6*-Gal4. Autophagosomes can be identified by the presence of both GFP and mCh fluorophores of this marker, whereas upon autophagosome–lysosome fusion the hybrid organelles become acidified, quenching the GFP fluorescence (Kimura et al., 2007). Within motoneurons, we observed both a cytoplasmic and punctate autophagosomal distribution of Atg8a. We found that autophagosome punctae (punctae double labeled with mCh and GFP) were present in the synaptic terminals of motoneurons (Fig. 1, B–B''), but were rarely found within the cell bodies (Fig. 1, D–D''). However, when lysosomal acidification was blocked by the depletion of a V-ATPase subunit, resulting in defective autolyosomes (Mauvezin et al., 2015), we observed a significant increase in the number of punctae in the cell body (Fig. 1, E–E'') but only a minor increase at synaptic terminals (Fig. 1, C–C''; and Fig. S1 A). These results suggest that autophagic vesicles acidify en route to the cell body. The distribution differences we see in these in situ experiments are similar to those reported for cultured dorsal root ganglion neurons (Maday et al., 2012). Our results suggest that autophagosomes that form at the synaptic terminals in *Drosophila* motoneurons in situ are transported toward the cell body and acidify as they move retrogradely.

To determine whether the minus end molecular motor complex cytoplasmic dynein mediates the transport of autophagosomes in *Drosophila* motoneurons, we monitored Atg8a localization when dynein was depleted. We observed that depletion of dynein subunits resulted in the accumulation of autophagosomes within the most distal bouton (terminal bouton) of synaptic terminals (dynein heavy chain 64c subunit RNAi; Fig. 1 G). In contrast, in control synaptic terminal autophagosomes were present but did not accumulate within terminal boutons of synaptic terminals at steady state (Fig. 1, B and F). To directly test whether the punctae that accumulate when dynein is depleted are autophagosomes, we simultaneously depleted dynein and disrupted the function of the autophagosome initiator kinase Atg1 by expression of a dominant-negative protein (Atg1 K38Q; Scott et al., 2007). We found that this significantly decreased the accumulation of autophagosomes (Fig. 1, H–J). Expression of dominant-negative $Atg1^{K38Q}$ alone shows a cytoplasmic distribution of Atg8a (Fig. 1 I). Collectively, these results support the role of the dynein motor complex in autophagosome transport for fusion with lysosomes.

Identification of CKA and its role in autophagic vesicle distribution at the synapse

We conducted an RNAi screen for *Drosophila* orthologues of human proteins that identified candidate regulators of autophagosome transport in neurons (see Materials and methods). Among the candidate proteins recovered was CKA, an orthologue of the mammalian striatin proteins (Chen et al., 2002). In humans, there are three striatin proteins, Striatin (Strn), Striatin 3 (Strn3, also known as SG2NA), and Striatin 4 (Strn4, also known as Zinedin), which are predominantly expressed in the brain (Castets et al., 2000). In *Drosophila*, zygotic *Cka*-null

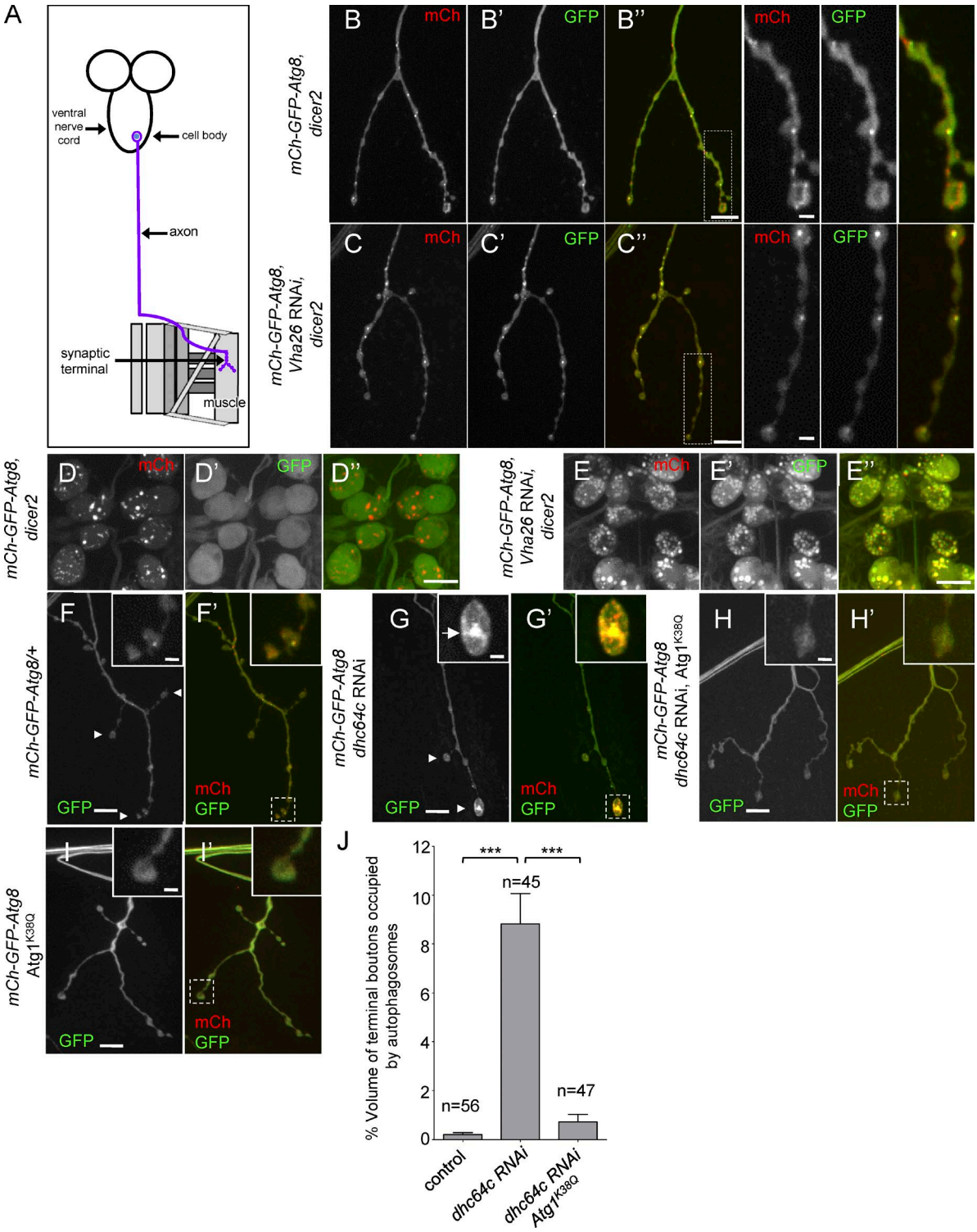

Figure 1. **Autophagosomes in *Drosophila* motoneurons in situ concentrate at synaptic terminals and are transported by dynein.** mCh-GFP-Atg8a protein was expressed in motoneurons using the *Ok6-Gal4* driver to observe the distribution of autophagosomes. (A) Diagram of the larval prep with the approximate location of motoneuron cell bodies, the NMJ at muscle 4, and the axon connecting the cell body and NMJ. (B–B'') Autophagosomes (double labeled with mCh and GFP) are observed in synaptic terminals of control larvae. (C–C'') When lysosomal acidification is blocked (*Vha26* RNAi), autophagosomes and defective autolysosomes are observed in synaptic terminals. The regions boxed in B'' and C'' are shown magnified to the right of the images. (D and E) Autophagosomes were rarely observed in cell bodies of motoneurons (D–D''), but defective autolysosomes were observed in cell bodies when lysosomal acidification is blocked (E–E''). (F and G) Synaptic terminals of controls did not accumulate autophagosomes within terminal boutons (F and F'), whereas autophagosomes accumulated when dynein was depleted (G and G'). The accumulation of autophagosomes is indicated by the arrow in the inset in G. Terminal boutons within the synaptic terminal are indicated by white arrowheads in F and G. (H and H') Disruption of the autophagy initiator kinase Atg1 largely suppressed the accumulation of autophagosomes in terminal boutons when dynein was depleted. (I and I') Autophagosome punctae are rarely present when Atg1 function is disrupted. The boxes in F', G', H', and I' are shown magnified as insets. (J) Percentage of terminal bouton volume occupied by autophagosomes. Data represent the mean and SEM. *n*, number of terminal boutons scored. Unpaired, two-tailed *t* test result: ***, $P < 0.0001$. Bars in magnified images and insets are 2 µm; all others are 10 µm.

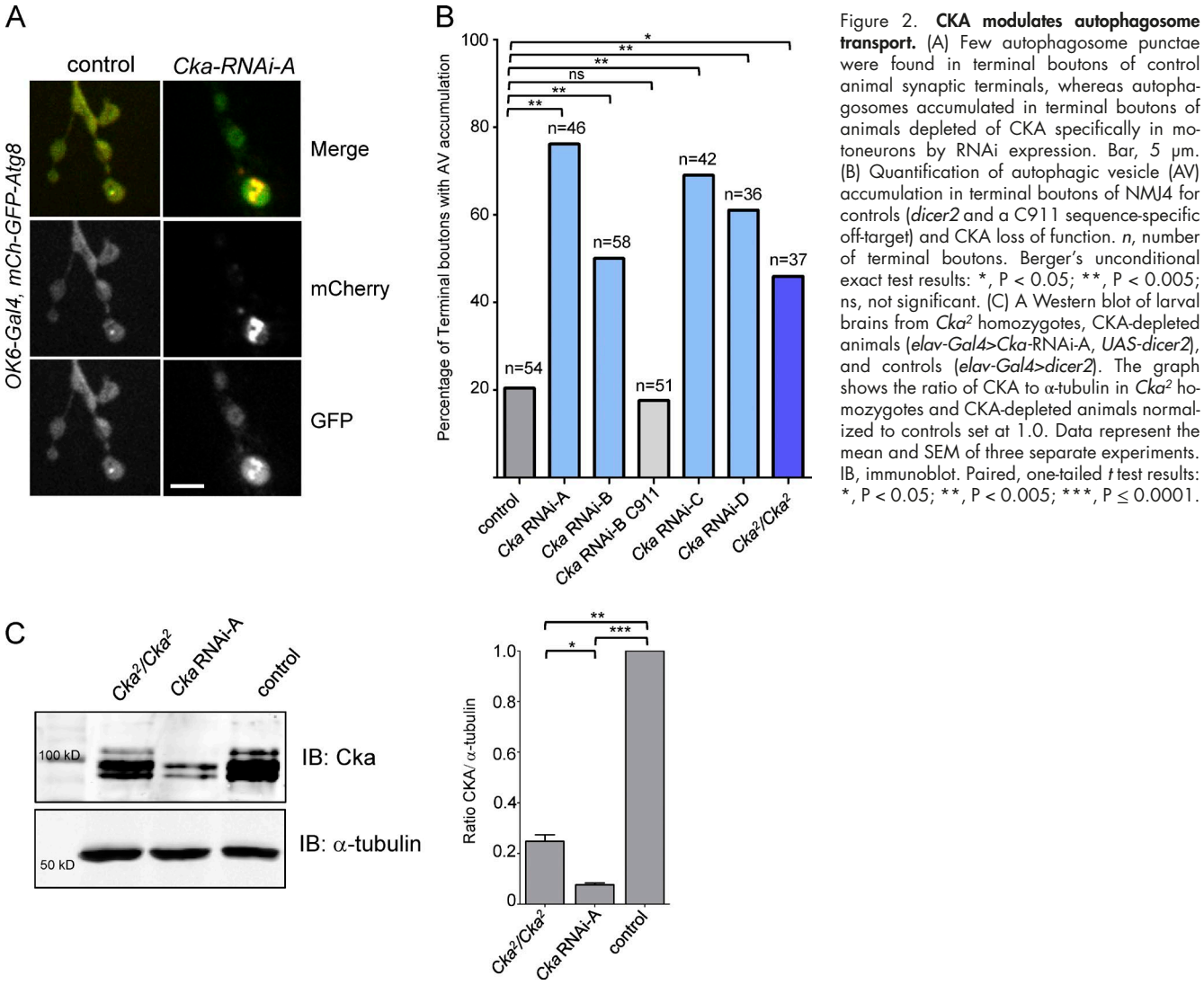

Figure 2. **CKA modulates autophagosome transport.** (A) Few autophagosome punctae were found in terminal boutons of control animal synaptic terminals, whereas autophagosomes accumulated in terminal boutons of animals depleted of CKA specifically in motoneurons by RNAi expression. Bar, 5 µm. (B) Quantification of autophagic vesicle (AV) accumulation in terminal boutons of NMJ4 for controls (*dicer2* and a C911 sequence-specific off-target) and CKA loss of function. *n*, number of terminal boutons. Berger's unconditional exact test results: *, $P < 0.05$; **, $P < 0.005$; ns, not significant. (C) A Western blot of larval brains from *Cka*^{2} homozygotes, CKA-depleted animals (*elav-Gal4>Cka*-RNAi-A, *UAS-dicer2*), and controls (*elav-Gal4>dicer2*). The graph shows the ratio of CKA to α-tubulin in *Cka*^{2} homozygotes and CKA-depleted animals normalized to controls set at 1.0. Data represent the mean and SEM of three separate experiments. IB, immunoblot. Paired, one-tailed *t* test results: *, $P < 0.05$; **, $P < 0.005$; ***, $P \leq 0.0001$.

mutants are pupal lethal (Chen et al., 2002), and we find that RNAi depletion of CKA specifically in neurons has a similar or earlier lethal developmental phase. Similar to dynein depletion, RNAi-mediated depletion of CKA in *Drosophila* motoneurons resulted in the accumulation of autophagosomes in terminal boutons (Fig. 2 A).

To quantify the transport defects that follow CKA depletion, *UAS-mCh-Atg8a* was expressed with the *D42-Gal4* neuronal driver, and synaptic terminals of neuromuscular junction 4 (NMJ4) were imaged by confocal microscopy. We scored changes in the number of terminal boutons that exhibited accumulations of autophagic vesicles after the depletion of CKA. We compared a control, four independent *Cka* RNAi lines, a sequence-specific RNAi off-target control (C911; Mohr et al., 2014), and homozygous *Cka*^{2}-null mutant animals (Chen et al., 2002). Depletion of CKA increased the percentage of terminal boutons that exhibit autophagic vesicle accumulation as compared with controls (Fig. 2 B). Interestingly, all of the *Cka* RNAi lines had a stronger accumulation phenotype than the homozygous *Cka*^{2}-null mutant. However, when we analyzed larval brains by Western blot, we found that the homozygous *Cka*^{2}-null mutants expressed more CKA protein than RNAi-depletion animals (Fig. 2 C). By Western blot, we observed at least three bands that may correspond to specific protein isoforms (Fig. S1 B) or may represent posttranslational modifications. In addition, most of the CKA protein in larval brains derives from neurons, not from glia, as RNAi depletion of CKA in glia had little impact on CKA levels in the brain (Fig. S1 C). We therefore inferred that perdurance of maternally loaded *Cka* mRNA contributes to the weaker accumulation phenotype in the motoneurons of *Cka*^{2} mutants. The observed differences in levels of CKA protein in *Cka*^{2} and *Cka* RNAi neurons suggest that an RNAi approach to gene identification may be more informative than a mutant clonal analysis in certain cell types such as neurons. Collectively, our observations support the notion that neuronal CKA protein regulates axonal autophagosome transport, and specifically the retrograde traffic from the synaptic terminal to the cell body.

CKA regulates autophagosome transport

To directly determine whether CKA depletion influences autophagosome transport, we performed live imaging of autophagosomes in motoneurons. *mCh-GFP-Atg8a* was expressed with *M12-Gal4*, which drives expression in two closely apposed motoneurons per segmental nerve (Xiong et al., 2010). Autophagosome motility was monitored in the mid-axon region of the two motoneurons. To selectively monitor autophagosomes, not autolysosomes, we tracked only organelles marked by the

GFP fluorescence of the mCh-GFP-Atg8a protein. In doing so, we found that there are strikingly few autophagosomes present within the mid-axon region of motoneurons (mean 1.0/axon pair in 2.5 min/108.36 µm; Fig. S2 A). To increase the number of autophagosomes for quantification, we used a mutation in *syntaxin17* (*syx17^{LL}*), an autophagosomal SNARE protein required for fusion with late endosomes/lysosomes. Blocking autophagosome–lysosome fusion increased the number of autophagosomes within the mid-axon region (mean 3.1/axon pair in 2.5 min/108.36 µm; Fig. S2 A). Interestingly, we found that autophagosomes in *Drosophila* motoneurons retained motility in the *syntaxin17* homozygous mutant background and exhibited motility dynamics similar to heterozygous *syx17^{LL}*/+ controls (Fig. S2 B). This is in contrast to studies in cultured dorsal root ganglion neurons, where autophagosomes are largely immotile after the depletion of syntaxin17 (Cheng et al., 2015). In the *syx17^{LL}/syx17^{LL}* genetic background in *Drosophila*, autophagosomes moved predominately in a retrograde fashion (88.8%), whereas very few moved anterograde (1.7%) or were stationary/nonprocessive (9.5%; Fig. 3, A and C). We observed a reduction in the number of autophagosomes in the axon after the depletion of either CKA or dynein in the *syx17^{LL}* mutant background (Fig. S2 A). Futhermore, when CKA was depleted in the *syx17^{LL}* mutant background using two independent RNAi lines, we observed a reduction in the percentages of retrograde autophagosomes (63.5% and 55%) and an increase in the percentages of anterograde (5.4% and 7.7%) and stationary/nonprocessive autophagosomes (31% and 36%; Fig. 3, A and C). A qualitatively similar but more pronounced effect was observed when dynein was depleted in the *syx17^{LL}* mutant background. The percentage of retrograde autophagosomes was diminished (24.6%), whereas the percentages of anterograde (7.7%) and stationary/nonprocessive autophagosomes (67.8%) were increased (Fig. 3 A). The retrograde flux of autophagosomes through the axon was significantly decreased when CKA or dynein was depleted (Fig. 3 B), whereas anterograde flux was only slightly increased (Fig. S2 C). These results demonstrate that CKA regulates autophagosome motility and does so in a manner similar to dynein. To assess whether CKA may function locally on autophagosomes, we asked whether a BFP-CKA protein colocalized with autophagosomes. We observed cotransport of BFP-CKA with GFP-Atg8a–labeled autophagosomes (Fig. 3 D), suggesting that CKA functions locally on autophagosomes to regulate their motility.

CKA forms a complex with dynein

To understand how CKA might regulate dynein-mediated transport of autophagosomes, we asked whether CKA resides in a complex with dynein. We found that GFP-CKA can bind and coimmunoprecipitate with endogenous dynein from cultured *Drosophila* cell extracts (Fig. 4, A and B). In addition, we show that endogenous Strip, a core component of STRIPAK, also coimmunoprecipitated with dynein (Fig. 4 C). *Drosophila* Strip directly binds to P150/Glued (Sakuma et al., 2014), which is a subunit of dynactin, an accessory complex to dynein. Potentially, CKA is in a complex with dynein/dynactin through its interaction with Strip. Previous work in mammalian cell extracts demonstrated that STRIPAK components complexed with cytoplasmic dynein (Goudreault et al., 2009), suggesting that these interactions are conserved across species. Collectively, these results suggest a molecular complex containing STRIPAK components is involved in the dynein/dynactin-mediated regulation of autophagosome transport.

CKA binds to Atg8 through a conserved LC3-interacting region (LIR) motif

We hypothesized that CKA functions as an adaptor protein in autophagosome transport, binding both the dynein motor complex and the autophagosome. In this model, Atg8a, an outer membrane protein of autophagosomes, mediates the CKA interaction. To test whether CKA links to autophagosomes by binding Atg8a, we conducted in vitro pull-down assays using bacterially expressed CKA protein and a GST-Atg8a fusion protein (or GST as a negative control). We found that the purified, full-length CKA bound directly to GST-Atg8a but not to GST (Fig. 5 B).

To determine the region of CKA required for the interaction with Atg8a, we first looked for known Atg8 interaction motifs within CKA. Atg8 interacts with numerous proteins through an LIR motif found in its binding partners. This Atg8/LIR interaction is essential for many steps in autophagy, including the selective targeting of organelles and proteins for autophagy, the regulation of autophagosome fusion, and the transport of autophagosomes (Pankiv et al., 2007, 2010; Fu et al., 2014; Lystad et al., 2014; Wong and Holzbaur, 2014a; McEwan et al., 2015). Using iLIR, a prediction software for LIR motifs (Kalvari et al., 2014), four LIR ([W/F/Y]-x-x-[L/I/V]) motifs were identified within CKA, three of which are conserved in Strn, Strn3, and Strn4 (Fig. 5 A). We next used a series of bacterially expressed CKA fusion proteins to determine the region required for Atg8a binding. An N-terminal fragment (CKA 1–466) as well as a C-terminal fragment (CKA 166–END) of CKA, both containing all three putative LIR motifs, pulled down with GST-Atg8a specifically (Fig. 5 B). Likewise, an N-terminal fragment (CKA 1–400) containing the first two LIR motifs pulled down specifically with GST-Atg8a. However, an N-terminal fragment containing only the first LIR motif (CKA 1–300) did not pull down with GST-Atg8a (Fig. 5 B).

Our domain analysis demonstrates that CKA and Atg8a interact directly and that the LIR2 domain between amino acids 300 and 400 is necessary for binding to Atg8a. To determine whether the CKA interaction with Atg8a depends on LIR2, we mutated both the phenylalanine (F) and leucine (L) within the LIR2 motif (FEFL) to alanine (A; CKA^{mutLIR2}) and assessed binding to GST-Atg8a. We conducted pull-down assays using a GFP-CKA or GFP-CKA^{mutLIR2} fusion protein expressed in cultured *Drosophila* cells. We found that the binding of GFP-CKA^{mutLIR2} to GST-Atg8a was diminished approximately twofold compared with wild-type GFP-CKA, whereas GST-Atg8a pulled down nearly identical levels of endogenous CKA protein in these experiments (Fig. 5 C). The dimerization of GFP-CKA^{mutLIR2} with endogenous CKA (Moreno et al., 2001; Chen et al., 2014) may account for the diminished binding. Consistent with this idea, we observed that GFP-CKA^{mutLIR2} coimmunoprecipitated with Flag-CKA (Fig. S3 A). Alternatively, a second region within CKA may contribute to its interaction with Atg8a. Similarly, MBP-Atg8a pulls down GFP-CKA, but not GFP-CKA^{mutLIR2} (Fig. S3 A). Based on these findings, we suggest that the LIR2 motif found within CKA in part mediates the interaction with Atg8.

A STRIPAK complex regulates autophagosome transport

To determine whether CKA's function in the axonal transport of autophagosomes is dependent on its function within the STRIPAK complex, we depleted the core components Strip, Mob4, and Ccm3 by RNAi and scored for autophagic vesicle accumulation in motoneuron terminal boutons. Similar to CKA,

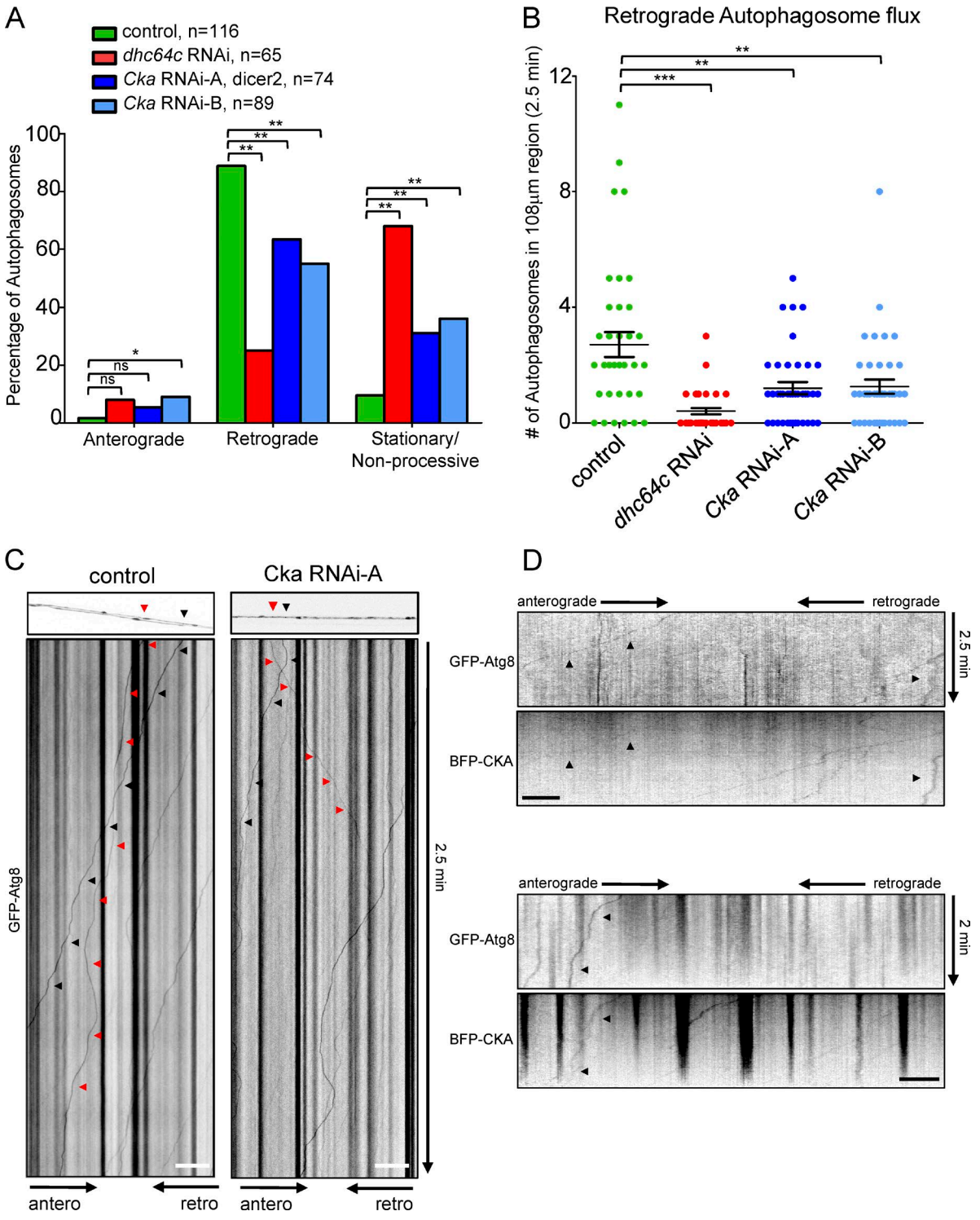

Figure 3. **CKA impacts autophagosome transport.** The motility of autophagosomes was tracked in the mid-axon region of motoneurons. All experiments were performed in an *syx17^{LL}/syx17^{LL}* background. Depletion of CKA affected autophagosome motility similar to the depletion of dynein. (A) Percentage of autophagosomes that had a net anterograde, net retrograde, or no motility for control, dynein depletion, and CKA depletion with two independent RNAi lines. *n*, number of autophagosomes scored. Berger's unconditional exact test results: *, P < 0.05; **, P < 0.005; ns, not significant. *n* = 39 axons for all except controls; *n* = 38 axons for controls. (B) Scatter plot of retrograde autophagosome flux measurements. Each point represents the analysis from one kymograph. Bars indicate the mean and SEM for each genotype. Unpaired, two-tailed *t* test results: **, P < 0.005; ***, P ≤ 0.0001. *n* = 39 axons for all except controls; *n* = 38 axons for controls. (C) Representative kymographs of autophagosome motility in the mid-axon region of control and *Cka* RNAi-A–depleted motoneurons. The box on top shows the axons at the start of imaging. Arrowheads indicate two autophagosomes present at the start of imaging for each genotype. The red arrowhead indicates the proximal autophagosome, whereas the black arrowhead indicates the distal autophagosome at the start of imaging, and these autophagosomes are tracked in the kymograph below. Bars, 20 µm. (D) Representative kymographs showing cotransport of BFP-CKA and GFP-Atg8. Endogenous CKA was depleted using the *Ok6-Gal4* driver in the *syx17^{LL}/syx17^{LL}* background. Arrowheads indicate punctae that are cotransporting. Bars, 10 µm.

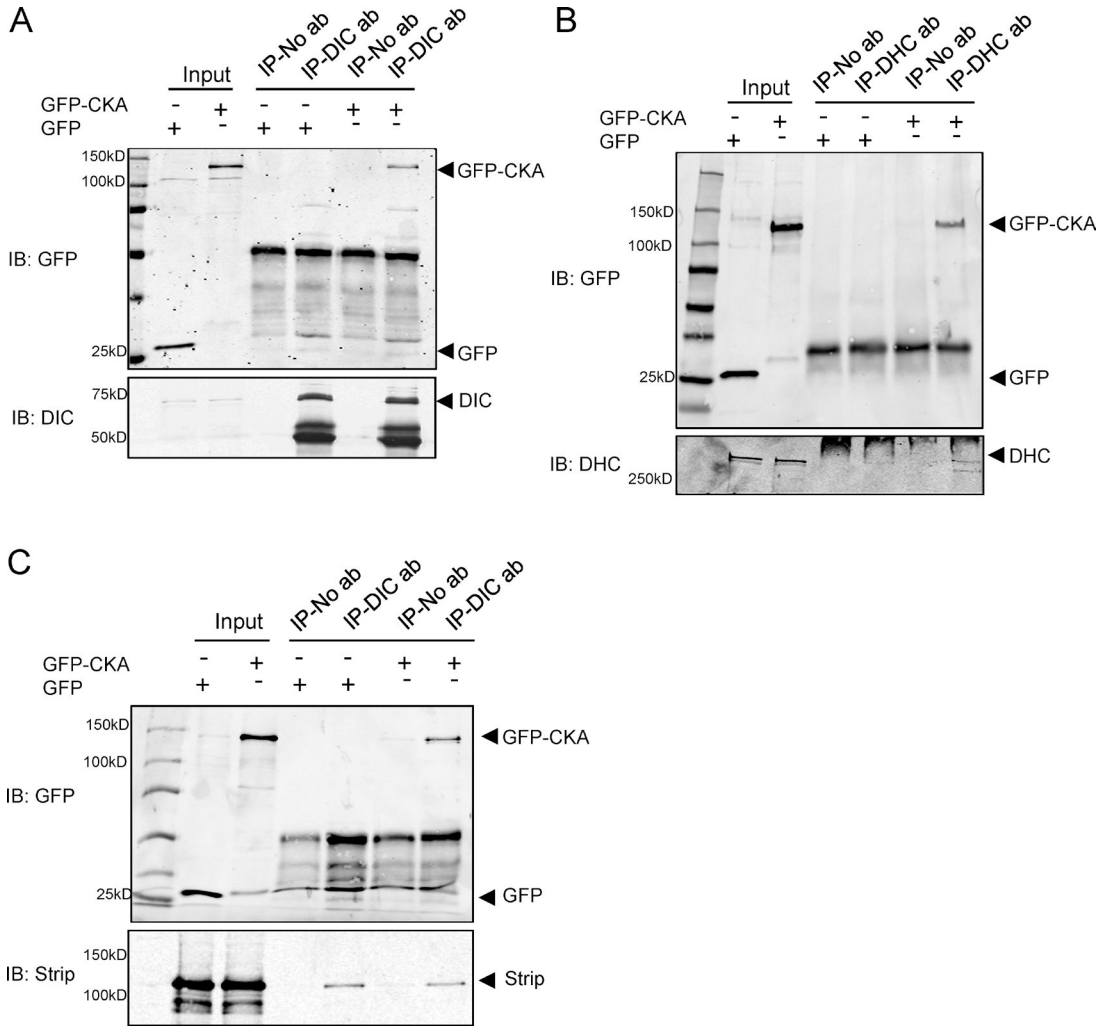

Figure 4. **CKA and Strip are in a complex with dynein.** (A and B) Immunoprecipitation of the dynein intermediate chain (DIC; A) or the dynein heavy chain (DHC; B) from cultured *Drosophila* cells expressing GFP or GFP-CKA demonstrated that GFP-CKA, but not GFP alone, coimmunoprecipitated with dynein. (C) Immunoprecipitation of the dynein intermediate chain from cultured *Drosophila* cells also coimmunoprecipitated endogenous Strip protein. Lysates were divided in half and put onto beads in the presence or absence (controls) of antibody. Representative blots are shown. IB, immunoblot; IP, immunoprecipitate. A and C, $n > 3$ repeats; B, $n = 2$ repeats.

animals depleted of Strip or Mob4 also exhibited a robust accumulation of autophagic vesicles in terminal boutons (Fig. 6 A). Significantly, we observed BFP-CKA punctae that cotransport with Cherry (Ch)-Mob4 punctae in motoneuron axons, suggesting that BFP-CKA incorporates into a complex that transports with autophagosomes (Fig. 6 B). In contrast, animals depleted of Ccm3 using three previously characterized RNAi lines (Song et al., 2013) showed no accumulation of autophagic vesicles in terminal boutons (Fig. 6 A). These results suggest that some, but not all, of the core STRIPAK complex components are involved in the regulation of autophagosome transport.

In both *Drosophila* and humans, the STRIPAK complex can associate with Hippo (Hpo) kinase (Ribeiro et al., 2010; Couzens et al., 2013; Liu et al., 2016). Moreover, in *Drosophila*, the STRIPAK complex acts to negatively regulate Hpo activity through the phosphatase PP2A (Ribeiro et al., 2010; Liu et al., 2016). To investigate the possibility that the STRIPAK complex modulates Hpo kinase activity to regulate autophagosome motility, we tested the epistatic relationship between Hpo and CKA. Whereas CKA depletion caused an accumulation of autophagic vesicles in terminal boutons, depletion of Hpo resulted in fewer terminal boutons with accumulated autophagic vesicles (Fig. 6 C), suggesting that CKA affects autophagosome motility through the negative regulation of Hpo. To test this hypothesis, we depleted both CKA and Hpo by RNAi and observed a reduction in the accumulation of autophagic vesicles compared with CKA depletion alone (Fig. 6 C). In addition, we found that the expression of *hpo* or hpo^{T195E}, a phosphomimetic in the Hpo activation loop, increased the accumulation of autophagic vesicles in terminal boutons compared with controls (Fig. 6 C). As the STRIPAK complex acts to negatively regulate Hpo activity, these results suggest that STRIPAK regulates autophagosome transport in part through the modulation of Hpo kinase activity.

STRIPAK components regulate transport of DCVs but not mitochondria

To investigate whether the STRIPAK complex has a broader role in organelle transport beyond autophagosomes, we monitored the flux of DCVs through the axon. We imaged DCVs in single neurons using the neuropeptide marker atrial natriuretic factor (ANF) fused to GFP (Rao et al., 2001) expressed with the *SG26.1-Gal4* driver (Gunawardena et al., 2003). After the

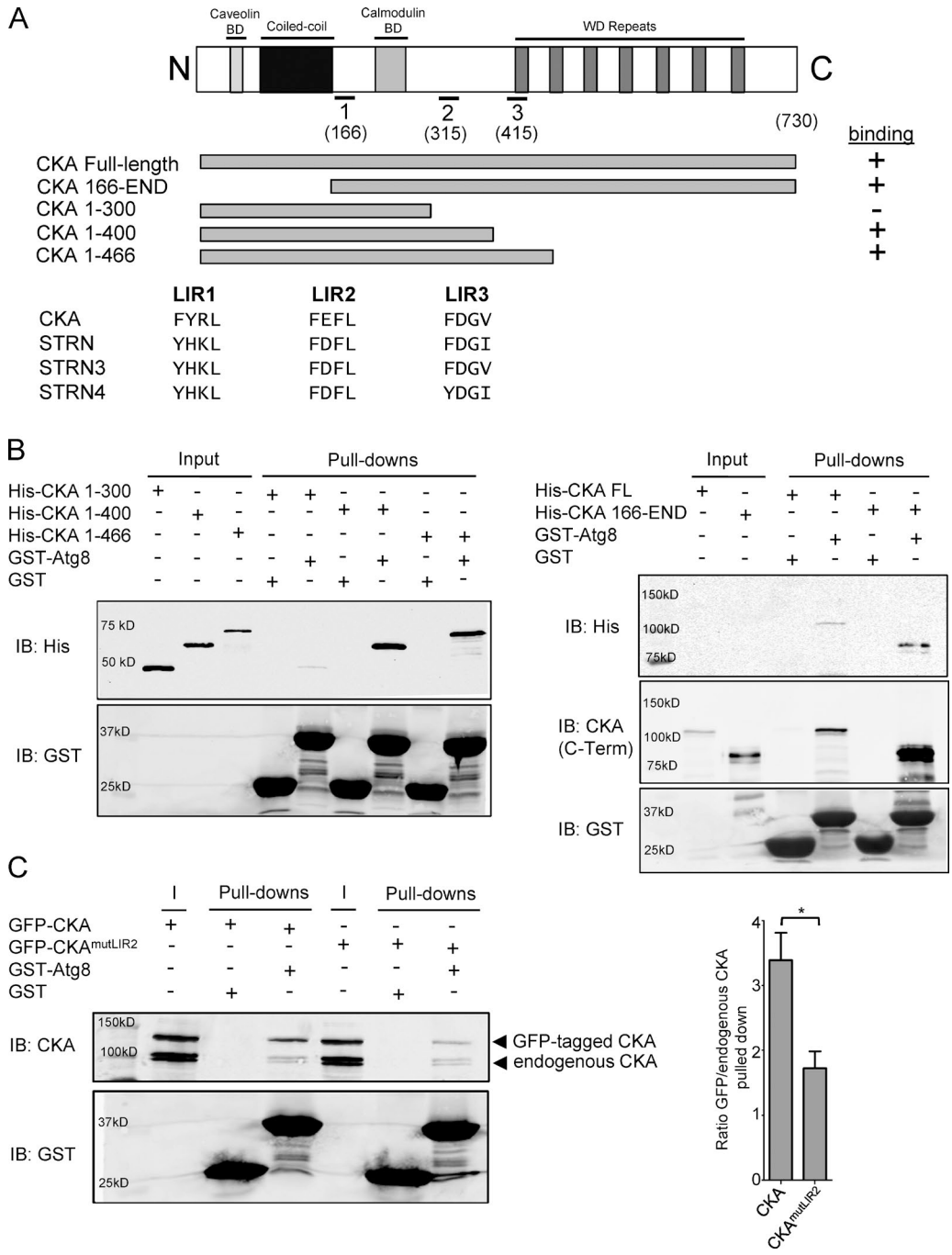

Figure 5. **CKA binds to Atg8 through a region containing a conserved LIR motif.** (A) Diagram of the CKA protein structure. Protein domains are indicated by boxes and labeled above the diagram. BD, binding domain. Three putative LIR motifs within CKA that are conserved in the mammalian striatin family orthologues are shown and denoted by a black line under the diagram with their amino acid coordinates. Bacterially expressed and purified protein fragments of CKA used for GST pull-downs are indicated under the diagram, and their binding ability to Atg8a is indicated to the right. (B) CKA directly bound to Atg8a through a region containing the LIR2 motif. All indicated protein fragments of CKA pulled down with GST-Atg8a except the N-terminal fragment that contains only the first LIR domain. (C) GFP-CKA and endogenous CKA from cultured *Drosophila* cells pulled down readily with GST-Atg8a, but not with GST alone. Mutating the LIR2 motif within CKA diminished the binding of GFP-CKA^{mutLIR2} to GST-Atg8a compared with GFP-CKA. Binding of endogenous CKA was similar between the GST-Atg8a pull-downs. The amount of GFP-CKA protein pulled down by GST-Atg8a normalized to endogenous CKA and GST-Atg8a protein levels for four separate experiments, and means and SEM are shown. IB, immunoblot. Paired, one-tailed *t* test results: *, $P < 0.05$. Representative blots are shown. For His pull-downs, CKA full-length, 1–300, and 1–400, $n \geq 3$ repeats; 1–466 and 166–END, $n = 2$ repeats.

depletion of the STRIPAK components or dynein, we observed a significant decrease in both the retrograde and anterograde flux of DCVs (Figs. 7 and S3 C). Furthermore, depletion of CKA, Mob, Strip, or dynein drastically decreased the number of DCVs found in the mid-axon region compared with controls (Figs. 7 and S3 D). In addition to the effects on DCV motility, we also noted that the depletion of STRIPAK components resulted in segmental nerve swellings that accumulated DCVs (*Cka* depletion; Fig. S3 D). Axon swellings and organelle jams in motoneurons are well-established phenotypes for dynein and

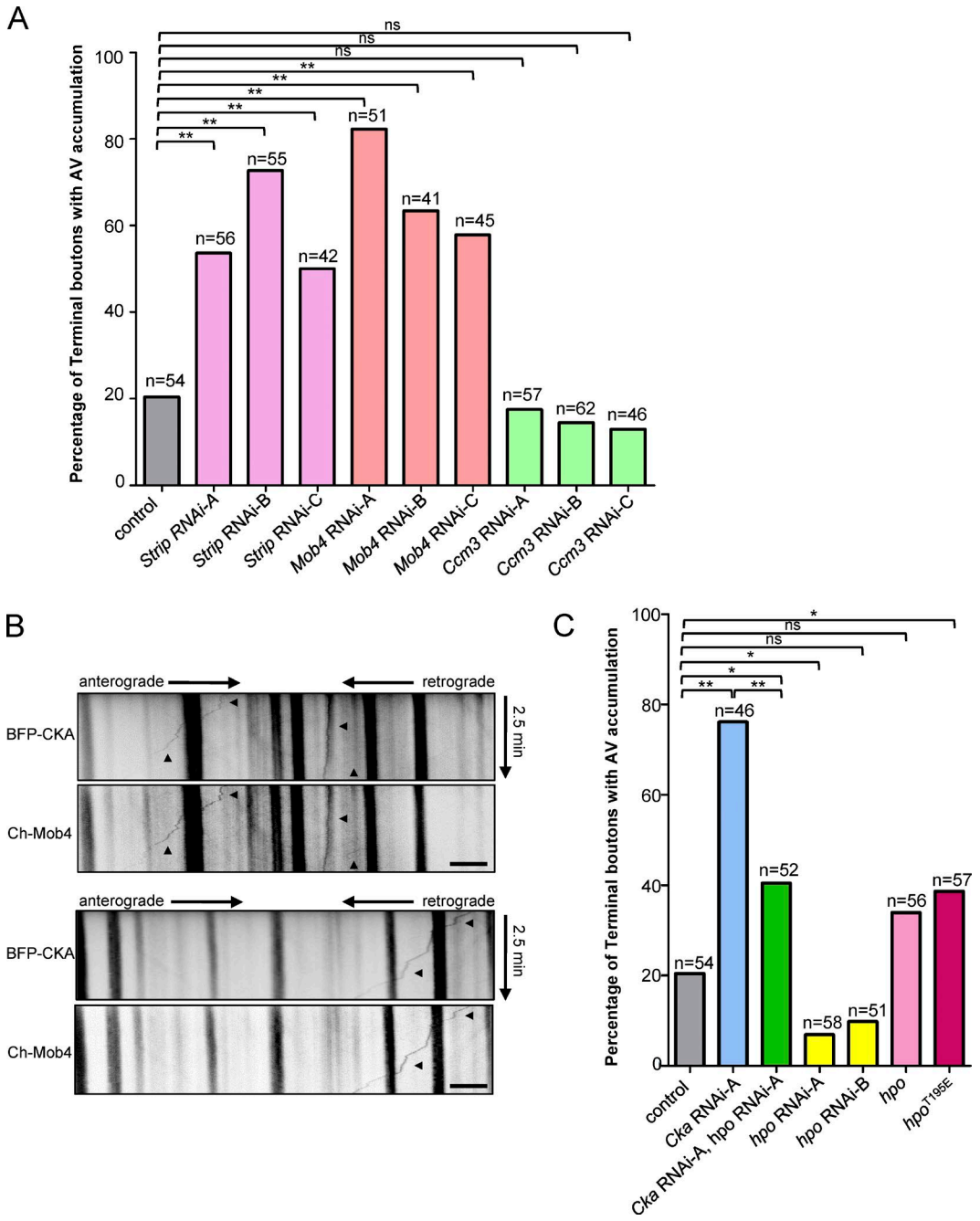

Figure 6. **A STRIPAK complex prevents autophagic vesicle accumulation.** (A) Quantification of autophagic vesicle (AV) accumulation in terminal boutons of NMJ4 when core STRIPAK components (Mob4, Strip, and Ccm3) were depleted in motoneurons. (B) BFP-CKA and Ch-Mob4 cotransport in axons. Arrowheads indicate punctae that are cotransporting. Bars, 10 µm. (C) Quantification of autophagic vesicle accumulation after expression of *hpo*, *hpo*^{T195E}, depletion of CKA alone, depletion of Hpo alone, or simultaneous depletion of Hpo and CKA. *n*, number of terminal boutons scored. Berger's unconditional exact test results: *, $P < 0.05$; **, $P < 0.005$; ns, not significant.

kinesin mutants, as well as for the JNK scaffolding proteins Jip3 and Jip1 in *Drosophila* (Hurd and Saxton, 1996; Martin et al., 1999; Bowman et al., 2000; Horiuchi et al., 2005). These results show that CKA, Mob4, and Strip can each participate in the transport of both autophagosomes and DCVs, suggesting that they function in concert to regulate vesicle motility.

To further test the specificity of the STRIPAK complex in organelle motility, we examined mitochondrial transport. The motility of mitochondria was monitored using the marker mito-GFP (Pilling et al., 2006) expressed with the *M12-Gal4* driver. To examine transport dynamics of mitochondria, we again measured the flux of mitochondria through the axon. The depletion of CKA, Mob4, or Strip did not decrease the flux of mitochondria in either direction (Figs. 8 and S4 A). By comparison, depletion of dynein significantly decreased mitochondrial flux in both directions (Figs. 8 and S4 A). Collectively, our results indicate that CKA, Mob4, and Strip differentially impact organelle transport. We suggest that STRIPAK components are resident on autophagosomes and DCVs, providing a local mechanism for regulating organelle transport.

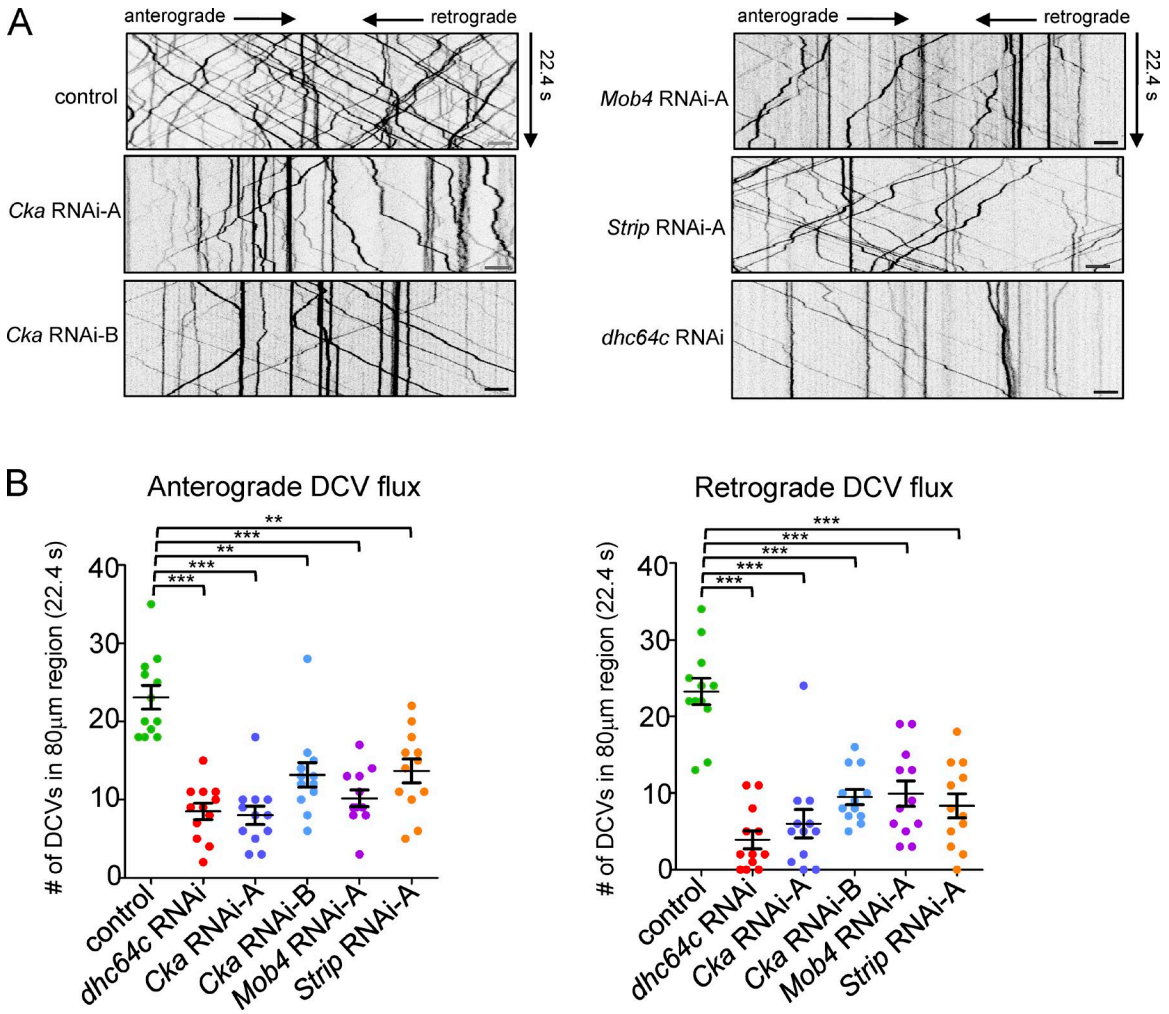

Figure 7. **A STRIPAK complex modulates the transport of DCVs.** (A) Representative kymographs of DCV motility for each of the genotypes measured. Bars, 5 µm. (B) Scatter plot of DCV flux measurements. Each point is the analysis from one kymograph. Bars indicate the mean and SEM for each genotype. The DCV flux in both directions was decreased when CKA, Mob4, Strip, or dynein were depleted. Unpaired, two-tailed *t* test result: **, $P < 0.005$; ***, $P \leq 0.0001$. $n = 12$ axons.

CKA/STRIPAK regulates motor-based transport through PP2A

CKA is a regulatory subunit of PP2A, and we next asked whether PP2A binding is important for CKA regulation of dynein-based motility. We generated constructs expressing a mutant CKA protein, $CKA^{\Delta PP2A}$, in which conserved residues necessary for PP2A binding (Gordon et al., 2011) were specifically mutated. We confirmed that these conserved residues mediate binding to the sole structural subunit of PP2A in *Drosophila*, Pp2A-29B. Coimmunoprecipitation experiments from *Drosophila* culture cells showed that GFP-CKA readily coimmunoprecipitate with Flag-tagged Pp2A-29B, but that the binding of the mutant GFP-$CKA^{\Delta PP2A}$ was diminished (Fig. S4 B).

To test the functional significance of this CKA–PP2A interaction, we made RNAi-resistant *BFP-Cka* and *BFP-*$Cka^{\Delta PP2A}$ transgenic lines to use in rescue experiments after the depletion of endogenous CKA. Both the control and mutant transgenes were inserted in the same genomic position to ensure comparable expression levels (Fig. S4 C). In the subsequent assessment of DCV motility, we found that the BFP-CKA protein provided partial rescue of the *Cka* RNAi transport defect, significantly increasing the retrograde flux of DCVs and slightly increasing DCV anterograde flux compared with deletion alone (Figs. 9 B and S4 D). In striking contrast, the mutant BFP-$CKA^{\Delta PP2A}$ protein did not rescue any of the defects in DCV flux observed after CKA depletion. The flux of retrograde and anterograde DCVs was significantly decreased compared with the depletion of CKA alone (Figs. 9 B and S4 D). These results suggest $CKA^{\Delta PP2A}$ may function in a dominant-negative fashion. To further support a role for PP2A in the regulation of transport, we similarly examined whether disruption of PP2A function impacts the accumulation of autophagic vesicles (Fig. 9, C and D). After depletion of the PP2A structural subunit, Pp2A-29B, we observed a significant increase in the accumulation of autophagic vesicles in terminal boutons (Fig. 9 C). By comparison, the depletion of the catalytic subunit (Mts) resulted in early lethality and prohibited an evaluation of the autophagosome accumulation. To circumvent this lethality, we used the conditionally inducible GeneSwitch system (Osterwalder et al., 2001) to deplete Mts by RNAi under the control of the *elavSwitch* driver. In this case, we observed a significant increase in the number of boutons with autophagic vesicle accumulation (Fig. 9 D). Depletion of Pp2A-29B by RNAi using the GeneSwitch system also resulted in a significantly greater number of boutons

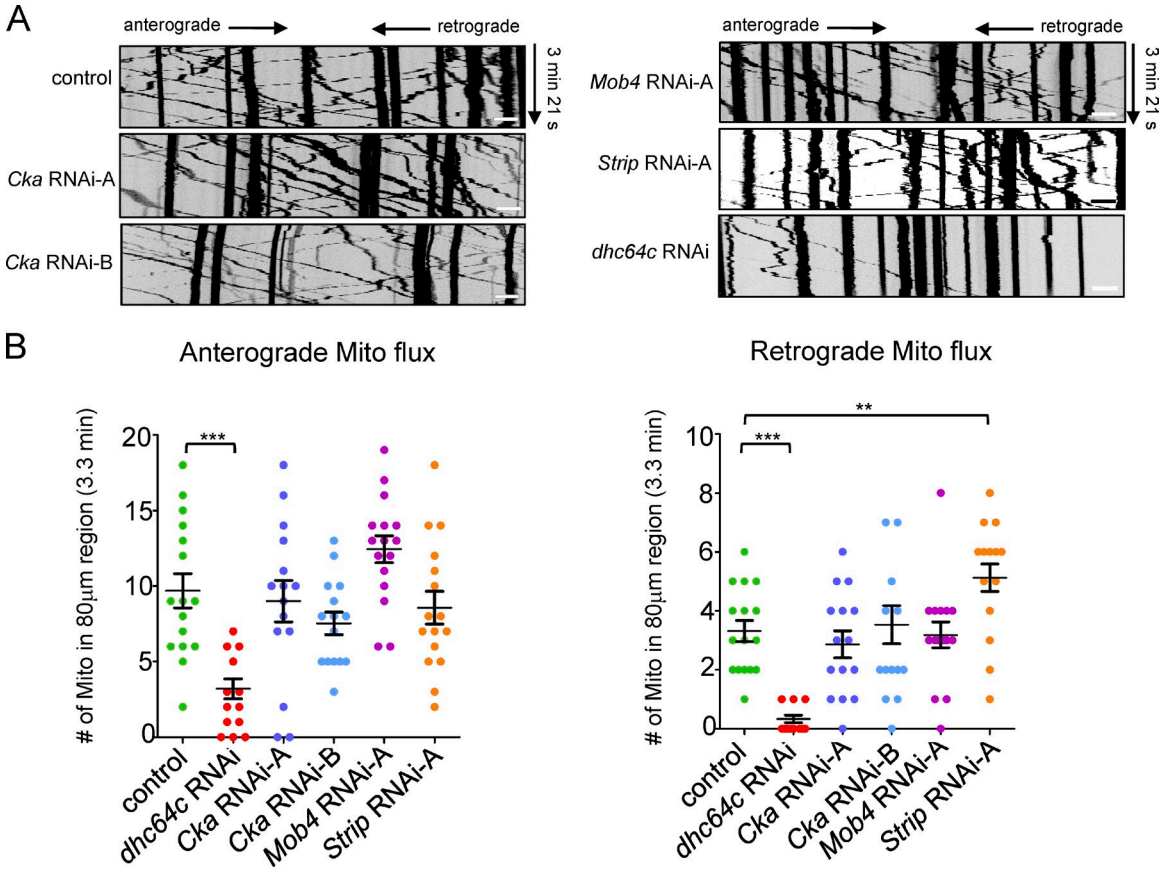

Figure 8. **A STRIPAK complex does not modulate mitochondrial transport.** (A) Representative kymographs of mitochondria motility for each of the genotypes measured. Bars, 5 µm. (B) Scatter plot of mitochondrial flux measurements. Each point is the analysis from one kymograph. Bars indicate the mean and SEM for each genotype. Depletion of CKA, Mob4, or Strip did not decrease the flux of mitochondria. Conversely, depletion of dynein decreases the flux of mitochondria in both directions. Unpaired, two-tailed *t* test results: **, $P < 0.005$; ***, $P \leq 0.0001$; all other comparisons to the control are not significant. $n = 15–16$ axons. Mito, mitochondria.

with accumulated autophagic vesicles (Fig. 9 D). Furthermore, we expressed a dominant-negative mutant form of the catalytic subunit (Mts^{DN}) that lacks the catalytic domain and retains the ability to incorporate into the STRIPAK complex (Evans et al., 1999; Hannus et al., 2002). Here, too, a significant increase in autophagic vesicle accumulation was observed using the conditionally inducible GeneSwitch system, supporting a requirement for PP2A catalytic activity in the regulation of motility (Fig. 9 D). In a parallel set of experiments, expression of Mts^{DN} or BFP-$CKA^{\Delta PP2A}$ under *D42-Gal4* resulted in increased autophagic vesicle accumulation, although this increase was not statistically significant (Fig. 9 C). The more modest effects may reflect a lower level of expression under the *D42-Gal4* driver. Nonetheless, collectively, our results support the interpretation that CKA and PP2A catalytic activity within the STRIPAK complex modulates axonal transport.

CKA itself may be regulated by associated kinase and PP2A activities. We found that CKA was hyperphosphorylated when cells were treated with okadaic acid, a PP2A inhibitor (Fig. 9 E), suggesting that CKA may be regulated by PP2A. Mammalian striatin proteins are also hyperphosphorylated when treated with okadaic acid (Moreno et al., 2001). To evalulate the presence of distinct CKA-phosphorylated species in cultured cell and larval brain extracts, we compared CKA immunoprecipitates on Western blots before and after treatment with λ-phosphatase. Without phosphatase treatment, we observed two CKA species in immunoprecipitates from cultured cells, and three species in immunoprecipitates recovered from larval brain lysates. Significantly, the number of bands remains the same after λ-phosphatase treatment (Fig. S4 E), suggesting there are multiple endogenous CKA isoforms that do not result from differential phosphorylation (Fig. S1 B). These results suggest that CKA itself is phosphoregulated and that, in addition, there are multiple endogenous CKA isoforms. The role of CKA phosphorylation and CKA isoform diversity in the regulation of transport remains to be elucidated.

To study the physiological consequence of depleting CKA in mature neurons, we used the neuronal *elav*-GeneSwitch driver (Osterwalder et al., 2001) to conditionally activate expression of the *Cka* RNAi construct late in development by feeding it the drug RU-486. To induce CKA depletion, we fed RU-486 to early third instar larvae and subsequently evaluated pupal eclosion rates and adult phenotypes. CKA depletion using the GeneSwitch system increased pupal lethality (reduced percentage of adults) compared with controls (Fig. 10 A). Significantly, all the CKA-depleted adults that eclosed were uncoordinated and exhibited very little movement (Fig. 10 A and Videos 1 and 2). Control adults raised on RU-486 food did not exhibit this uncoordinated locomotor phenotype (Fig. 10 A and Video 3). Moreover, the uncoordinated adult phenotype observed after CKA depletion could be substantially rescued by BFP-CKA fusion protein

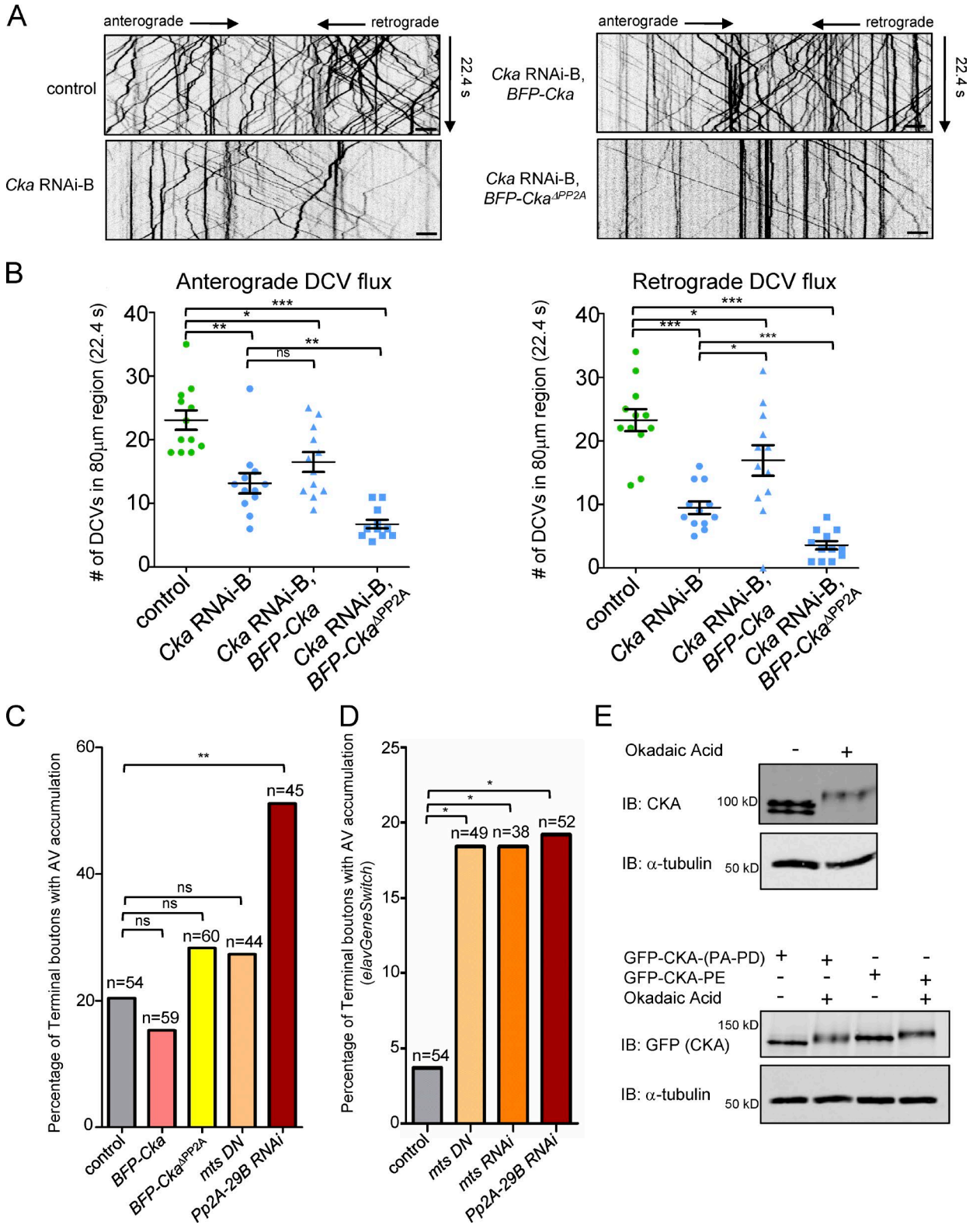

Figure 9. **PP2A binding to CKA is required for DCV motility.** (A) Representative kymographs of DCV motility for each of the genotypes measured. Bars, 5 µm. (B) Scatter plot of DCV flux measurements. Each point is the analysis from one kymograph. Bars indicate the mean and SEM for each genotype. BFP-CKA expression after CKA depletion significantly rescued the retrograde flux of DCVs and increased the anterograde flux of DCVs. In contrast, expression of a BFP-CKA fusion protein that cannot bind PP2A (BFP-CKA$^{\Delta PP2A}$) after CKA depletion significantly reduced the flux of DCVs in both directions compared with CKA depletion alone. Unpaired, two-tailed *t* test result: *, $P < 0.05$; **, $P < 0.005$; ***, $P \leq 0.0001$; ns, not significant. $n = 12$ axons. (C) Quantification of autophagic vesicle (AV) accumulation in terminal boutons of NMJ4 when *BFP-Cka*, *BFP-Cka*$^{\Delta PP2A}$, *mts*^{DN}, or *Pp2A-29B* RNAi were expressed. (D) Quantification of autophagic vesicle accumulation in terminal boutons of NMJ4 when PP2A activity is disrupted using the *elav*-GeneSwitch driver. Berger's unconditional exact test results: *, $P < 0.05$; **, $P < 0.005$; ns, not significant. (E) A phospho shift of endogenous CKA and GFP-tagged CKA isoforms was seen when cells were treated with okadaic acid, a PP2A inhibitor. Representative blots are shown. IB, immunoblot. $n = 2$ repeats.

A

Genotype	# Larvae	# Pupae	# Adults	Uncoordinated?
Cka RNAi-B C911 (control) ETOH	300	287 (95.7%)	282 (98.3%)	0%
Cka RNA-B C911 (control) RU-486	300	289 (96.3%)	282 (98.3%)	0%
Cka RNAi-B ETOH	300	283 (94.3%)	277 (97.9%)	0%
Cka RNAi-B RU-486	300	289 (96.3%)	236 (81.6%)	100%
Cka RNAi-B, *BFP-Cka* ETOH	300	283 (94.3%)	279 (98.6%)	0%
Cka RNAi-B, *BFP-Cka* RU-486	300	284 (94.7%)	281 (98.9%)	0%
Cka RNAi-B, *BFP-Cka*$^{\Delta PP2A}$ ETOH	300	277 (92.3%)	270 (97.5%)	0%
Cka RNAi-B, *BFP-Cka*$^{\Delta PP2A}$ RU-486	300	283 (94.3%)	163 (57.6%)	100%

B

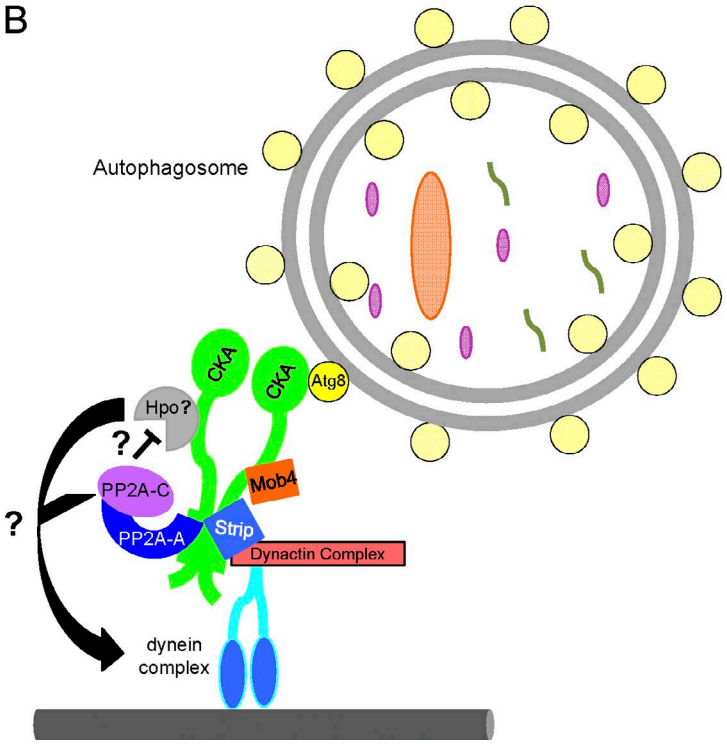

Figure 10. **CKA is required for adult motor coordination.** (A) Effect of depletion of CKA in late larval brains on viability and adult motor coordination. Expression of transgenes in late larval stages was controlled by feeding RU-486. Loss of neuronal CKA late in development has a minor effect on viability but results in a pronounced uncoordinated phenotype. This phenotype is rescued by BFP-CKA but not BFP-CKA$^{\Delta PP2A}$ expression. (B) A model for the function of a STRIPAK complex in axonal transport. CKA functions as a scaffold protein, binding core STRIPAK components Mob4, Strip, and the structural subunit PP2A (A), as well as kinases. Strip binds directly to the P150 subunit of the dynactin complex (Sakuma et al., 2014). Dynactin is a regulatory complex of dynein, and the dynein/dynactin association is necessary for retrograde transport. CKA binds directly to Atg8a, a protein that localizes to the membrane of autophagosomes. As a core STRIPAK component, CKA mediates attachment of autophagosomes to dynein/dynactin transport machinery. The STRIPAK complex also tethers PP2A and kinases that may coregulate the dynein-mediated transport of a subset of organelles.

expression (Fig. 10 A and Video 4). Importantly, the uncoordinated locomotor phenotype was not rescued by the mutant BFP-CKA$^{\Delta PP2A}$ fusion protein (Fig. 10 A and Videos 5 and 6). In addition, an increase in pupal lethality was observed when BFP-CKA$^{\Delta PP2A}$ fusion protein was expressed in neurons depleted of endogenous CKA (Fig. 10 A), again supporting the conclusion that the BFP-CKA$^{\Delta PP2A}$ mutant protein functions as a dominant-negative inhibitor of CKA function. Collectively, these results demonstrate that CKA's function within the nervous system is dependent on PP2A activity and is required for coordinated locomotion in adult *Drosophila*.

Discussion

Autophagy plays an important role in neuronal homeostasis, removing misfolded proteins and damaged organelles that compromise neuronal function. To our knowledge, this is the first study of the distribution and dynamics of autophagosomes in *Drosophila* motoneurons in situ. We find that autophagosomes in neurons with established synaptic connections are primarily found within synaptic terminals and are rarely seen in motoneuron cell bodies. These autophagosomes move predominantly in a retrograde direction and are powered by the dynein motor,

similar to the autophagosome dynamics described in cultured mammalian neurons (Maday et al., 2012; Cheng et al., 2015). We performed an RNAi-based screen and identified the striatin family protein CKA as a regulator of autophagosome transport.

CKA is a core component of the STRIPAK complex and scaffolds the phosphatase PP2A, kinases, and additional protein components, including Mob4 and Strip. We report that the STRIPAK complex plays a broad role in axonal transport, regulating the transport of autophagosomes and DCVs. Moreover, although the flux of both autophagosomes and DCVs through the axon is decreased by the depletion of STRIPAK components, mitochondrial transport is largely unaffected. This suggests that the STRIPAK complex has specificity in the regulation of organelle transport. Other work has suggested that the STRIPAK components Strip and Mob4 act globally to regulate microtubule stability and organization, potentially through the posttranslational modification of tubulin and microtubule-associated proteins (Schulte et al., 2010; Sakuma et al., 2015). Moreover, in *Drosophila* Strip and Mob4 mutants, defects in neuronal and synaptic morphologies have been observed and could arise as the downstream consequences of microtubule dysregulation (Schulte et al., 2010; Sakuma et al., 2014). Axonal aggregates and larval motility defects were also reported in Mob4 mutants, but whether these defects reflect a disruption of microtubule organization or the aberrant regulation of motor proteins was not addressed (Schulte et al., 2010). Our observations of the differential impact of STRIPAK depletion in organelle transport are not readily explained by global defects in microtubule stability or microtubule organization and point to a specific defect in organelle transport regulation.

Our data suggest a model in which the STRIPAK complex acts as a molecular linker between autophagosomes and the dynein motor complex. We show that CKA directly binds the autophagosomal membrane protein Atg8a and, similar to the mammalian STRIPAK complex (Goudreault et al., 2009), also associates with cytoplasmic dynein. However, we cannot exclude the possibility that CKA/STRIPAK acts as a cofactor in the regulation of dynein. Further work will be required to understand the role of CKA in the attachment and regulation of motor proteins. In addition, our genetic and motility data further suggest that the STRIPAK complex acts to regulate dynein-based transport in neurons through phosphoregulation events. We hypothesize that dynein and dynein-associated proteins are likely substrates. Previous work by many groups has demonstrated that dynein subunits and dynein-associated proteins are phosphorylated. These phosphorylation events can modulate interactions between dynein, its regulators, or attached cargoes (Vaughan et al., 2001; Pandey and Smith, 2011; Mitchell et al., 2012; Gao et al., 2015; Klinman and Holzbaur, 2015; Nirschl et al., 2016), influencing transport or the initial loading of cargo. Previous work has shown that the loading of cargoes into the microtubule is dependent on retrograde machinery, including the dynein/dynactin complex (Lloyd et al., 2012; Moughamian and Holzbaur, 2012). Here, we find that autophagosomes accumulate at synaptic terminals after the depletion of CKA, suggesting a related regulatory role for CKA activity in dynein-mediated microtubule attachment in neurons.

Beyond acting as a putative molecular linker, we demonstrate that the CKA scaffold tethers the phosphatase PP2A, which modulates axonal transport. Previous studies have shown that PP2A regulatory subunits, including CKA, control PP2A phosphatase activity in a diverse array of cellular functions in *Drosophila* (Viquez et al., 2006; Wang et al., 2009, 2016; Ribeiro et al., 2010; Bose et al., 2014; Li et al., 2014; Andreazza et al., 2015; Sun and Buttitta, 2015; Swarup et al., 2015). In motoneurons, disruption of all PP2A activities results in multiple neuronal phenotypes, including axonal transport defects (Viquez et al., 2009). Our data support a model in which CKA is the PP2A-regulatory subunit that controls axonal transport. Depletion of CKA and PP2A exhibits similar axonal transport defect phenotypes. Moreover, we show that a BFP-CKA fusion protein partially rescues the DCV motility phenotype observed when CKA is depleted, whereas expression of BFP-CKA$^{\Delta PP2A}$, a mutant with greatly reduced PP2A binding capability, cannot rescue the DCV motility defects. A role in axonal transport has not been described for any of the other regulatory subunits in *Drosophila*. *Well-rounded*, another PP2A regulatory subunit, is known to regulate synaptic growth, cytoskeletal stability (Viquez et al., 2006), and active zone stability but does not affect axonal transport (Li et al., 2014). In light of these observations, we propose that CKA not only acts as a linker to bridge autophagosomes to the dynein motor complex, but also regulates axonal transport through the modulation of PP2A phosphatase activity.

CKA likely scaffolds both PP2A and the kinase that functions in opposition to PP2A to regulate the phosphorylation of proteins required for retrograde dynein-mediated axonal transport (Fig. 10 B). The opposing action of kinases and phosphatases serves to finely tune substrate activity in multiple cellular processes. For example, in *Drosophila*, GSK3β kinase acts in opposition to PP2A to coordinately regulate substrates (Viquez et al., 2009; Li et al., 2014). In addition to defects in axonal transport, aberrant cytoskeletal organization and defective development of synaptic active zones are observed after loss of PP2A activity in *Drosophila* motoneurons. Significantly, the active zone and cytoskeletal phenotypes are suppressed by a reduction in the level of GSK3β (Viquez et al., 2009). In contrast, no suppression of the axonal transport defects was reported, suggesting that GSK3β is not the kinase that acts with PP2A to regulate axonal transport. Instead, the axonal transport defects and vesicle accumulations are more severe if both PP2A and GSK3β are reduced (Viquez et al., 2009). The increased severity may reflect the involvement of GSK3β in negatively regulating both kinesin-1 and dynein to coordinate bidirectional transport in neurons (Weaver et al., 2013). These results suggest that another kinase, yet unidentified, functions in opposition to PP2A activity to regulate axonal transport. Our results suggest that Hpo is the candidate STRIPAK kinase that mediates autophagosome transport. Future work will seek to identify the STRIPAK-associated kinases in neurons and their substrates in neurons. Regardless of the identity of the STRIPAK-associated kinase, our work has linked the STRIPAK complex and its core PP2A regulatory subunit, CKA, to the transport of autophagosomes and DCVs in neurons. These results raise the possibility that dysregulation of axonal transport could underlie the previously reported linkage between PP2A dysfunction, tau hyperphosphorylation, synaptic deficits, and Alzheimer's disease (Gong et al., 1993; Rudrabhatla, 2014; Sontag and Sontag, 2014). In support of this possibility, our work demonstrates that depletion of CKA results in a severe neurological phenotype in adult *Drosophila*.

The STRIPAK complex has recently been implicated in the regulation of a broad range of cellular processes (Ribeiro et al., 2010; Kean et al., 2011; Hyodo et al., 2012; Hwang and Pallas, 2014; Andreazza et al., 2015; Lant et al., 2015). An

important question is how the STRIPAK complex is targeted to specific functions and whether redundant regulatory mechanisms exist. The components of the STRIPAK complex have been identified in cultured mammalian (Goudreault et al., 2009) and *Drosophila* (Ribeiro et al., 2010) cells, but functional investigations of the heterogeneity in subunit composition are only just beginning. In the present study, we find that in *Drosophila* motoneurons, not all core components of the STRIPAK complex contribute to the regulation of organelle motility. Specifically, depletion of Ccm3 had no effect on autophagosome transport, suggesting that Ccm3 is either not in the STRIPAK complex in motoneurons or does not function within the complex to regulate axonal transport. In mammalian cells, Ccm3 bridges striatin and the kinase GckIII within the STRIPAK complex (Kean et al., 2011). Consistent with the idea that Ccm3 function is not required for autophagosome transport, we also found that depletion or overexpression of GckIII did not impact the autophagosome distribution in neurons (unpublished data). Future work will explore the tissue and functional specificity for components in the STRIPAK complex. Moreover, in addition to CKA/STRIPAK, the scaffolding complexes Huntingtin/HAP1 and JIP1 are also known to impact the transport of autophagosomes in neurons (Fu et al., 2014; Wong and Holzbaur, 2014b). In a similar fashion to CKA, JIP1 binds and coregulates JNKs (Yasuda et al., 1999; Horiuchi et al., 2007) and the phosphatase MKP7 (Willoughby et al., 2003), impacting the transport of numerous organelles and vesicles (Matsuda et al., 2001; Scheinfeld et al., 2002; Horiuchi et al., 2005; Fu et al., 2014). Remarkably, JIP1 also binds to the Atg8 orthologue LC3 through an LIR motif (Fu et al., 2014). The fact that multiple scaffolding proteins modulate autophagosome transport raises many interesting questions regarding the targeting of scaffolding proteins to distinct subpopulations of autophagosomes. Alternatively, the redundancy of scaffolding complexes involved in autophagosome transport may help ensure the clearing of cellular debris to safeguard neuronal homeostasis and function.

Materials and methods

Drosophila stocks

Table S1 lists the genotypes used to evalulate the data for each experiment. Flies were raised on standard food, and all crosses were performed at 29°C. Stocks used are as follows: *UAS-mito-GFP* (Pilling et al., 2006), *UAS-ANF-GFP* (Rao et al., 2001), *UAS-mCh-GFP-Atg8a* (Takáts et al., 2013), *UAS-mCh-Atg8a* (Chang and Neufeld, 2009), *UAS-Atg1^{K38Q}[13A]/TM6,Tb* (Scott et al., 2007), *syx17^{LL}/TM6,Tb* (Hegedűs et al., 2013), *Cka^{2}/Cyo* (a gift from S. Hou, National Cancer Institute, Frederick, MD; Chen et al., 2002), *UAS-Flag-hpo* and *UAS-Flag-hpo^{T195E}* (a gift from L. Zhang and Y. Jin, Shanghai Institutes for Biological Sciences, Shanghai, China; Jin et al., 2012), *Ok6*-Gal4 (Aberle et al., 2002), *D42*-Gal4 (Bloomington Drosophila Stock Center [BDSC]), *M12*-Gal4 (Xiong et al., 2010), *SG26.1*-Gal4 (Gunawardena et al., 2003), and *UAS-mts^{DN}* (Mts 1–181; Hannus et al., 2002). Vienna Drosophila Resource Center (VDRC) RNAi lines used are as follows: *UAS-dhc64cRNAi* (28054), *UAS-CkaRNAi*-A (106971), *UAS-CkaRNAi*-C (35234), *UAS-Mob4RNAi*-A (110742), *UAS-Mob4RNAi*-C (40442), *UAS-StripRNAi*-A (106184), *UAS-StripRNAi*-B (16211), *Ccm3RNAi*-A (109453), *Ccm3RNAi*-B (46548), *Ccm3RNAi*-C (106841), *vha26*RNAi (102378), and *UAS-hpoRNAi-B* (104169). Lines from the BDSC were as follows: *UAS-CkaRNAi*-D (*Cka^{HM05138}*), *UAS-Mob4RNAi*-B (*UAS-Mob4RNAi.JS1*), *UAS-StripRNAi*-C (*Strip^{HMS01134}*), *UAS-hpo*RNAi-A (*hpo^{HMS00006}*), *UAS-Pp2A-29BRNAi* (*pP2A-29B^{JF03316}*), *UAS-mtsRNAi* (*mts^{JF02805}*), *elav-Switch.O*, and *UAS-Mob4-N*-Cherry. The wild-type outcross control was *w^{1118}* unless indicated otherwise.

Larval dissections

Wandering third instar larvae were dissected in HL3 saline (70 mM NaCl, 5 mM KCl, 20 mM $MgCl_2$, 10 mM $NaHCO_3$, 5 mM trehalose, 115 mM sucrose, and 5 mM Hepes, pH 7.2) by filleting the larva open on an imaging platform of a custom-made Sylgard dish according to the procedure described by Neisch et al. (2016). All imaging was done on live, freshly dissected larvae in HL3 saline except for images of DCV segmental nerve axonal jams. These animals were dissected as described above, fixed in 4% paraformaldehyde for 20 min, and then washed in PBS before mounting in Prolong gold antifade (Molecular Probes).

RNAi screen to identify candidate proteins

Proteins conserved between humans and *Drosophila* were identified using InParanoid7 (Ostlund et al., 2010). Proteins were depleted by crossing VDRC RNAi lines to a recombinant *Ok6Gal4, UAS-mCh-GFP-Atg8a*; *UAS-dicer2/TM6,Tb.* Three larvae for each genotype were dissected. Dissected animals were visually screened for terminal bouton accumulation of autophagosomes by epifluorescence microscopy using a Plan-Apo 60×/1.4 NA oil objective on an Eclipse T*i* microscope (Nikon). Full results from this screen will be reported separately.

Imaging of autophagosome distribution and analysis

An *Ok-Gal4, UAS-mCh-GFP-Atg8a; UAS-dicer2/TM6,Tb* line was crossed to *UAS-vha26-RNAi* or *w^{1118}*. Images of mCh and GFP within cell bodies and synaptic terminals were obtained with a C-Apo 63×/1.2 NA water immersion objective (Olympus). A microscope (Axio Observer Z1; ZEISS) equipped with a spinning-disk confocal head (CSU-X1; Yokogawa Electric Corporation) and QuantEM 512SC camera (Photometrics) was used along with Zen2 software (ZEISS) for acquisition. NMJ4 synaptic terminals within abdominal segments A4 and A5 were imaged for five animals of each genotype. The images were then compiled as a SUM projection in FIJI (ImageJ; National Institutes of Health) and randomized using the filename randomizer ImageJ macro, written by Tiago Ferreira. Images were then scored blind by counting the number of GFP puncta in each synaptic terminal. 20 synaptic terminals were analyzed for each genotype.

Imaging of autophagosome accumulation in terminal boutons and volumetric analysis

An *Ok-Gal4, UAS-mCh-GFP-Atg8a* line was crossed to *w^{1118}*, and *UAS-dhc64cRNAi* or *Ok-Gal4, UAS-mCh-GFP-Atg8a/Cyo-dfd-YFP; UAS-dhc64cRNAi/TM6,tubGal80,Tb* was crossed to *UAS-Atg1^{K38Q}* (Scott et al., 2007). mCh and GFP within synaptic terminals of NMJ4 within abdominal segments A2–A5 were imaged for three animals of each genotype. 17 synaptic terminals of *dhc64c* RNAi, 20 synaptic terminals of controls, and 17 synaptic terminals of *dhc64c* RNAi, *Atg1^{K38Q}* were imaged. Samples were imaged with a spinning-disk confocal microscope (ZEISS) and randomized as described in the previous section. Imaris software (Bitplane) was used to create a volumetric reconstruction of the synaptic terminals. The mCh signal was used to create a mask of the synaptic terminal to calculate the volume of the terminal boutons. The GFP signal was then used to identify autophagosome punctae and determine the volume they occupied in the terminal bouton. As signal intensity was variable for each image, the threshold was manually adjusted, and signal was only counted as GFP puncta if visually present.

Imaging of autophagic vesicle accumulation in terminal boutons and analysis

A *D42-Gal4, UAS-mCh-Atg8a, UAS-dicer2* recombinant line was crossed to the indicated RNAi lines, or a *Cka*^{2}*; D42-Gal4, UAS-mCh-Atg8a/SM5-TM6,Tb* line was crossed to *Cka*^{2}*/SM5-TM6,Tb* (Chen et al., 2002). mCh signal in synaptic terminals of NMJ4 within abdominal segments A4 and A5 was imaged for each of the given genotypes with a Plan-Apo 63×/1.4 NA oil immersion objective and a spinning-disk confocal microscope (ZEISS; see Imaging of autophagosome distribution and analysis section). Z stacks were collected by imaging from just above to just below the synaptic terminal using identical settings. 23–26 synaptic terminals from six to seven animals were imaged, except for *StripRNAi-C* (20 synaptic terminals and five animals) and *Cka*^{2} mutants (16 terminals and four animals). The number of terminal boutons varied per synaptic terminal. The images were then compiled as a SUM projection in FIJI and randomized as decribed in the Imaging of autophagosome distribution and analysis section above. A minimum of six genotypes and a least 146 images were randomized together for analysis each time. The images were then scored for terminal bouton accumulation. Autophagosomes at synaptic terminals had a mean diameter of 0.5 µm. The smallest terminal boutons analyzed were 1.5 µm in diameter. Terminal boutons were counted as having accumulation if >20% of the bouton had signal above the cytoplasmic signal observed in the more proximal boutons. The terminal boutons within each synapse were visually scored as having or lacking an accumulation of autophagic vesicles. Berger's unconditional two-sided exact test was used to analyze the data (Berger, 1996a,b).

Imaging of autophagic vesicle accumulation in terminal boutons using *elav*-GeneSwitch

A *UAS-mCh-GFP-Atg8a; elavSwitch.O* line was crossed to the indicated RNAi or dominant-negative transgenic animals. The *elav*-GeneSwitch driver was used to conditionally express mCh-GFP-Atg8a while depleting the PP2A catalytic or structural subunits by RNAi. Alternatively, the *elav*-GeneSwitch was used to conditionally express the dominant-negative catalytic subunit (Mts^{DN}) in neurons. Expression was induced by feeding first instar larvae the drug RU-486. Embryos were collected on juice plates at 25°C. First instar larvae were transferred to food containing 20 µg/ml mifepristone (RU-486; Sigma-Aldrich) dissolved in 100% EtOH. Larvae were then raised at 29°C. Synaptic terminals of NMJ4 were then imaged and analyzed as described in the Imaging of autophagosome distribution and analysis section. 22–26 synaptic terminals from six to seven animals were imaged. At least three genotypes and 68 images were randomized together for analysis. Berger's unconditional two-sided exact test was used to analyze the data (Berger, 1996a,b).

Autophagosome motility imaging and analysis

An *M12-Gal4, UAS-mCh-GFP-Atg8a, syx17*^{LL}*/TM6,Tb* line was crossed to *syx17*^{LL}*/TM6,Tb* (Hegedűs et al., 2013), *UAS-CkaRNAi-A; UAS-dicer2, syx17*^{LL}*/TM6,Tb, UAS-CkaRNAi-B; syx17*^{LL}*/TM6,Tb,* or *UAS-dhc64cRNAi, syx17*^{LL}*/TM6,Tb*. GFP signal in the mid-axon region of motoneurons was imaged at a distance 800–1,000 µm from the ventral nerve cord (VNC) with a C-Apo 63×/1.2 NA water immersion objective on a spinning-disk confocal microscope (ZEISS; as described in the Imaging of autophagosome distribution and analysis section). Images were obtained continuously for 2.5 min using Zen software (ZEISS). Images were then analyzed by making kymographs using MetaMorph software (7.7.10.0; Molecular Devices). Autophagosomes were classified as having a net movement in the retrograde direction, anterograde direction, stationary, or no net displacement (nonmotile). Nonmotile autophagosomes were identified by watching the video to identify autophagosomes at time 0 and track those that were nonmotile in the kymograph, as changes in axon width accumulate cytosolic Atg8a and appear as straight lines in kymographs. Seven animals of each genotype were used. 39 axons were imaged for *Cka* RNAi-A, *Cka* RNAi-B, *dhc64c* RNAi, and *syx17*^{LL}/+, and 38 axons were imaged for controls (*syx17*^{LL}*/syx17*^{LL}). Prism 5 software (GraphPad Software) was used to graph the resulting data. Berger's unconditional two-sided exact test was used to analyze the data (Berger, 1996a,b).

Imaging autophagosome cotransport with BFP-CKA

An *Ok6-Gal4, UAS-mCh-GFP-Atg8*; *syx17*^{LL}*/TM6,Tb* line was crossed to a *UAS-Cka-RNAi-B; UAS-BFP-Cka, syx17*^{LL}*/TM6,Tb* line. GFP and BFP signals in the mid-axon region of motoneurons were imaged at a distance 800–1,000 µm from the VNC with a C-Apo 63×/1.2 NA water immersion objective on a spinning-disk confocal microscope (ZEISS; as described in the Imaging of autophagosome distribution and analysis section). Exposure times used were BFP, 300 ms, and GFP, 150 ms. Images were obtained with sequential, continuous aquisition for 2–2.5 min using Zen software. Images were then analyzed by making kymographs using MetaMorph software.

Imaging Ch-Mob4 cotransport with BFP-CKA

An *SG26.1-Gal4, UAS-Ch-Mob4* line was crossed to a *UAS-Cka-RNAi-B; UAS-BFP-Cka* line. BFP and Ch signals in the mid-axon region of motoneurons were imaged at a distance 800–1,000 µm from the VNC with a C-Apo 63×/1.2 NA water immersion objective on a spinning disk confocal microscope (ZEISS; as described in the Imaging of autophagosome distribution and analysis section). Exposure times used were BFP, 300 ms, and Ch, 100 ms. Images were obtained with sequential, continuous aquisition for 2.5 min using Zen software. Images were then analyzed by making kymographs using MetaMorph software.

Imaging and analysis of DCV motility

An *SG26.1-Gal4, UAS-ANF-GFP* line was crossed to the indicated RNAi lines. *Cka*RNAi-A, *Mob4*RNAi-A, and *Strip*RNAi-A lines carried *UAS-dicer2* to increase RNAi efficiency. GFP was imaged within the mid-axon region of motoneurons at a distance 800–1,000 µm from the VNC with an Apo TIRF 100×/1.49 NA oil immersion objective. A microscope (Eclipse T*i*) equipped with a spinning-disk confocal head (Wallac Ultraview; BioProcess) and an electron-multiplying charge-coupled device camera (Evolve 512; Photometrics) was used for acquisition. Images were obtained using MetaMorph software and acquired using continuous streaming. Images were then analyzed by making kymographs of 150 frames (22.4 s). Two axons were analyzed from six animals of each genotype (12 axons total). The number of retrograde and anterograde DCVs within the 80-µm region over a 22.4-s period was counted. Prism 5 software was used to run unpaired, two-tailed *t* tests for analysis of statistically significant differences.

Imaging of DCV axonal jams

The posterior portion of synaptic nerves containing axonal jams was imaged 1,000–2,000 µm from the VNC with a Plan-Apo 63×/1.4 NA oil immersion objective on a spinning-disk confocal microscope (ZEISS).

Imaging and analysis of mitochondria motility

An *M12-Gal4, UAS-GFP-HA-mito* line was crossed to the indicated RNAi lines. *Cka*RNAi-A, *Mob4*RNAi-A, and *Strip*RNAi-A lines carried *UAS-dicer2* to increase RNAi efficiency. Expression of *UAS-dicer2* was used as the control. The mid-axon region of motoneurons was imaged at a distance 800–1,000 µm from the VNC with an Apo total internal reflection flurescence 100×/1.49 NA oil immersion objective on a Nikon microscope and MetaMorph software (as described

in the Imaging and analysis of DCV motility section). Images were acquired every 2 s for 100 frames (3 min, 21 s). Three to four axons were analyzed from four animals of each genotype (15–16 axons total). The number of retrograde and anterograde mitochondria within the 80-µm region over a period of 3 min 21 s was counted. Prism 5 software was used to run unpaired, two-tailed *t* tests for analysis of statistically significant differences.

Expression constructs

GFP-CKA corresponding to isoforms PA, PB, PC, and PD was used for all cultured cell experiments except the Flag-CKA coimmunoprecipitate of GFP-CKA, which corresponded to isoform PE. To make pUAST-*EGFP-Cka* (corresponding to CKA protein isforms PA, PB, PC, and PD), *Cka* was digested out of pCEFL-*Cka* (a gift from S. Hou) with BamHI–XbaI, and *EGFP* was PCR amplified to incorporate 5′ EcoRI–3′ BamHI sites for digestion. Both the *Cka* and *EGFP* fragments were subcloned into pBS KS$^+$ cut with EcoRI–XbaI. *EGFP-Cka* was then subcloned out of pBS KS$^+$ and into pUASTattB by an EcoRI digest, and the orientation was confirmed. To make pUAST-*EGFP-Cka* (corresponding to CKA-PE), *Cka* was PCR amplified from the cDNA clone MIP15828 (obtained from the Drosophila Genomic Resource Center) to incorporate a 5′ BamHI and 3′ NotI site. This was subcloned into pUASTattB cut with EcoRI–NotI along with the *EGFP* fragment cut with EcoRI–BamHI. The resulting clone was sequence verified. To create the pUAST-*EGFP-Cka^{mutLIR2}* and pUAST-*EGFP-Cka$^{\Delta PP2A}$* mutant constructs, PCR site-directed mutagenesis was used on the pBS KS$^+$ *EGFP-Cka* clones (corresponding to protein isoforms PA-PD and PE) to mutate the phenylalanine (F) 315 and leucine (L) 318 within the FxxL LIR motif to alanine (A) or to mutate the arginine (R) 150 and 151 to serine (S) or glutamate (E), respectively. The resulting clone was verified by sequencing and subcloned out of pBS KS$^+$ and into pUASTattB by an EcoRI digest. The orientation of the insert was confirmed. To create the *Flag–Pp2A-29B* construct, the RE28669 EST clone (Bloomington Drosophila Genome Project) was used. PCR site-directed mutagenesis was used to add a basepair (cytosine) at 917 that was missing in the clone. *Pp2A-29B* was then PCR amplified to incorporate a 5′ NotI and 3′ XbaI site. The *Pp2A-29B* PCR product was digested with NotI–XbaI and subcloned into the pUASTattB 3×Flag vector (Mauvezin et al., 2016) cut with the same enzymes. The resulting clone was verified by sequence analysis. To create the *Flag-Cka* construct (corresponding to the CKA-PE isoform), *Cka* was PCR amplified from the BFP-*Cka* clones containing a mutated 3′ UTR (described in the BFP-*Cka* fly lines section) *Cka* to incorporate 5′ and 3′ NotI sites. The resulting PCR product was digested with NotI and subcloned into the pUASTattB 3×Flag vector (Mauvezin et al., 2016) cut with the same enzymes. The orientation was verified and the clone was fully sequenced.

Cka RNAi-B line and *Cka* RNAi-C911

To create a *Cka* RNAi line against a shared region of the *Cka* 3′ UTR, oligonucleotides were used to make an shRNA. The oligonucleotides were 5′-CTAGCAGTGCGAGTTCGAGTTAAATAATTTAGTTATATTCAAGCATAAATTATTTAACTCGAACTCGCGCG-3′ and 5′-AATTCGCGCGAGTTCGAGTTAAATAATTTATGCTTGAATATAACTAAATTATTTAACTCGAACTCGCACTG-3′. To create the shRNA *Cka* RNAi-C911 off-target control line (Mohr et al., 2014), replacing bases 9–11 with their complementary bases to destroy perfect matching to *Cka* but leaving the siRNA seed region intact, the oligonucleotides were 5′-CTAGCAGTGCGAGTTCGACAAAAATAATTTAGTTATATTCAAGCATAAATTATTTTTGTCGAACTCGCGCG-3′ and 5′-AATTCGCGCGAGTTCGACAAAAATAATTTATGCTTGAATATAACTAAATTATTTTTGTCGAACTCGCACTG-3′. The pairs of oligonucleotides were annealed in buffer containing 10 mM Tris-HCl, pH 6.5, 0.1 M NaCl, and 1 mM EDTA, and the annealed product was digested with NheI–EcoRI and cloned into pValium20 (DF/HCC Plasmid Resource Core) digested with the same enzymes. The resulting clone was verified by sequencing. PhiC31 integrase-mediated transgenesis was used to generate transgenic lines using the attP40 site by BestGene Inc.

BFP-*Cka* fly lines

To create the *UAS-BFP-Cka* and *UAS-BFP-Cka$^{\Delta PP2A}$* fly lines, the cDNA clone MIP15828 (corresponding to CKA protein isoform PE) was obtained from the Drosophila Genomic Resource Center, and *Cka* was PCR amplified to retain the 3′ UTR sequence, incorporating 5′ BamHI and 3′ NotI sites. This PCR product was then subcloned into the pBS KS$^+$ vector after digesting with BamHI–NotI. The resulting clone was used to mutate the PP2A binding site in CKA (changing amino acids R150S and R151E) using site-directed mutagenesis. *BFP* was PCR amplified to incorporate a 5′ EcoRI site and 3′ BamHI site from fly DNA obtained from the fly stock (*lexAop-UAS-TagBFP.CAAX.k) 77B/TM6B,Tb*; Bloomington Drosophila Stock Center). *Cka* and *Cka$^{\Delta PP2A}$* were subcloned out of pBS KS$^+$ by a BamHI–NotI digest and subcloned into the pUASTattB vector digested with EcoRI–NotI along with the BFP PCR product digested with EcoRI–BamHI. The resulting clones of pUASTattB-*BFP-Cka* and pUASTattB-*BFP-Cka$^{\Delta PP2A}$* were sequence verified. The 3′ UTR sequence of the pBS KS$^+$ *Cka* clone was mutated to change 9 of the 21 base pairs targeted by the *CkaRNAi-B* shRNA line. An NdeI–NotI fragment containing the mutated 3′ UTR was then subcloned into the pUASTattB-*BFP-Cka* and pUASTattB-*BFP-Cka$^{\Delta PP2A}$* constructs that had been digested with NdeI–NotI to remove the original 3′ UTR sequence. At each step in the subcloning process, the resulting clone was verified by sequencing. PhiC31 integrase-mediated transgenesis was used to generate transgenic lines using the attP2 site by BestGene Inc.

GST fusion proteins

Atg8a was PCR amplified from pUAST-*mCh-Atg8a* adult fly genomic DNA to incorporate 5′ BamHI and 3′ XhoI sites. This PCR product was then subcloned into pGEX-KText vector digested with the same enzymes. The resulting clone was sequence verified. GST and GST-Atg8a (pGEX-KText and pGEX-KText-*Atg8a*) proteins were expressed and purified from BL21 cells in salty TE buffer (150 mM NaCl, 10 mM Tris, pH 8.0, and 1 mM EDTA, pH 8.0) containing 0.2 mg/ml lysozyme, CellLytic B (Sigma-Aldrich), 50 U/ml benzonase nuclease (Sigma-Aldrich), and EDTA-free cOmplete protease inhibitor cocktail (Roche) and bound to glutathione Sepharose 4B beads (GE Healthcare).

MBP fusion proteins

Atg8a was digested out of pGEX-KText-*Atg8a* using a BamHI–XhoI digest and subcloned into the pMAL-cRI vector digested with BamHI–SalI. The resulting clone was verified by a BamHI–PstI digest. MBP and MBP-Atg8a (pMAL-cRI and pMAL-cRI-Atg8a) were expressed and purified from BL21 cells in salty TE buffer containing 10 mg/ml lysozyme, 50 U/ml benzonase nuclease, and EDTA-free cOmplete mini protease inhibitor cocktail and bound to amylose resin (New England Biolabs, Inc.).

SUMO-6×His fusion proteins

Full-length *Cka* and *Cka* fragments were PCR amplified using pUAST-*EGFP-Cka* (corresponding to protein isoforms PA, PB, PC, and PD) as a template, with primers to incorporate 5′ AarI and 3′ XbaI sites and, when necessary, a start codon (CKA 166–END) or stop codon (CKA 1–300, CKA 1–400, and/or CKA 1–466). These PCR products were then digested with AarI and XbaI and subcloned into the pE-SUMO

vector digested with BsaI. The resulting clones were sequence verified. SUMO-6×His fusion proteins were expressed and purified from BL21 cells in salty TE buffer containing 20 mM imidazole, pH 7.5, CellLytic B, and 50 U/ml benzonase and bound to nickel–nitrilotriacetic acid agarose beads (QIAGEN). The fusion proteins were eluted off in salty TE buffer containing 200 mM imidazole, pH 7.5.

Immunoprecipitations

For dynein coimmunoprecipitation experiments, 8.0×10^6 S2 cells were transfected with *actin-Gal4* and *UAS-EGFP-Cka* using dimethyldioctadecyl-ammonium bromide (Sigma-Aldrich) at 250 µg/ml 2 d after transfection. Cells were harvested and lysed in PMEG buffer containing 100 mM Pipes, 5 mM MgOAc, 5 mM EGTA, 0.1 mM EDTA, 0.5 mM DTT, 0.9 M glycerol, 0.1% Triton X-100, and EDTA-free cOmplete protease inhibitor cocktail. Immunoprecipitation reactions were performed at 4°C for 2 h. Antibodies used for immunoprecipitations were mouse anti-dynein intermediate chain (74.1; EMD Millipore) and mouse anti-dynein heavy chain, P1H4 (McGrail and Hays, 1997). For Flag-Pp2A coimmunoprecipitation experiments, S2 cells were transfected with actin-Gal4 and *UAS-3×Flag–Pp2A-29B* with *UAS-GFP-Cka*, or *UAS-GFP-Cka*^{LIR2}, or *UAS-GFP-Cka*$^{\Delta PP2A}$, and *UAS-Cka*RNAi-B and *Cka* double-stranded RNA as described above for cell transfections of *actin-Gal4* and *UAS-EGFP-Cka*. Flag immunoprecipitations were performed using Flag M2 agarose beads (Sigma-Aldrich) 2 d after transfection. Cells were harvested and lysed in a buffer containing 50 mM Hepes, 150 mM NaCl, 0.5 mM EGTA, 0.9 M glycerol, 0.1% Triton X-100, 0.5 mM DTT, and EDTA-free cOmplete protease inhibitor cocktail. Immunoprecipitation reactions were performed at 4°C for 2 h. 2% of the input of each reaction was loaded onto the gel.

GST pull-downs

For GST pull-downs of S2 cell lysates, 8.0×10^6 S2 cells were transfected with *actin-Gal4* and *UAS-EGFP-Cka* or *UAS-EGFP-Cka*^{mutLIR2}. 2 d after transfection, cells were lysed in the buffer used for immunoprecipitations with 1% Triton X-100. Lysates were divided in half and put onto GST- or GST-Atg8a–bound beads. Binding reactions were performed at 4°C for 2 h. 2% of the input for each reaction was loaded onto the gel. For GST pull-downs of purified fusion proteins, eluted fusion proteins were diluted in salty TE buffer with a final concentration of 0.1% Triton X-100. An equal concentration of imidazole was maintained in all reactions being compared. Equal volumes of protein samples were put onto GST- or GST-Atg8a–bound beads. Binding reactions were performed at 4°C for 2 h. 3% of the input of each reaction was loaded onto the gel.

Larval brain lysates

Third instar wandering larval brains were dissected in PBS and lysed directly in 1× SDS protein gel sample buffer containing EDTA-free cOmplete protease inhibitor cocktail. Per every 15 brains, 20 µl of buffer was used for lysis. Lysis was performed by pipeting the sample up and down and then boiling for 5 min. 10 brain equivalents were loaded per well per genotype.

λ-phosphatase treatment

S2 cells were plated at a density of 8.0×10^6 cells and used 2 d later for immunoprecipitation of endogenous CKA using a rabbit anti-CKA antibody (a gift from W. Du, University of Chicago, Chicago, IL). As a control, cells were transfected with pAc-*Myc-hpo* (Wu et al., 2003) and pAGW-*yki* (actin promoter, N-terminal GFP tag; a gift from R. Fehon, University of Chicago, Chicago, IL) and immunoprecipitated using a rabbit anti-GFP antibody (Molecular Probes). 140 late third instar larval brains were dissected in PBS and used for immunoprecipitation of endogenous CKA using a rabbit anti-CKA antibody (a gift from W. Du). The lysis buffer used was as follows: 50 mM Hepes, 150 mM NaCl, 0.5 mM EGTA, 0.9 M glycerol, 0.1% Triton X-100, 0.5 mM DTT, EDTA-free cOmplete protease inhibitor cocktail, and PhosSTOP protein phosphatase inhibitors (Sigma-Aldrich). Immunoprecipitation reactions were performed at 4°C for 2 h. Immunoprecipitation reations were washed twice with 1× NEBuffer for protein metallophosphotases (New England Biolabs, Inc.) containing 1 mM $MnCl_2$ before λ-phosphatase treatment. The bead volume was split in half, and half the beads were treated with 400 U λ-phosphatase (New England Biolabs, Inc.) at 30°C for 45 min.

Okadaic acid treatment

S2 cells were plated at a density of 2.7×10^6 cells and transfected with *actin-Gal4* and *UAS-GFP-Cka* (corresponding to CKA PA-PD or CKA-PE) or were untransfected. 2 d after plating, cells were treated for 3 h with 1 µM okadaic acid in DMSO or the same volume of DMSO. Cells were then harvested and lysed in 2× SDS protein sample buffer.

Immunoblotting

7.5% or 10% SDS-PAGE gels or 4–15% mini-PROTEAN TGX gels (Bio-Rad Laboratories) were transferred onto nitrocellulose. Antibodies were used at the following concentrations: rabbit anti-CKA, 1:2,000 (a gift from W. Du); mouse anti–α-tubulin, 1:2,000 (DM1A; Sigma-Aldrich); goat anti-GST, 1:1,000 (Pharmacia); mouse anti-poly-His, 1:3,000 (HIS-1; Sigma-Aldrich); rabbit anti-GFP, 1:2,000 (Molecular Probes); rat anti-Strip, 1:500 (a gift from T. Chihara, University of Tokyo, Tokyo, Japan); mouse anti-dynein intermediate chain, 1:2,000; mouse anti-Flag, 1:20,000 (M2; Sigma-Aldrich); and rabbit anti-tRFP, 1:1,667 (recognizes TagBFP; Evrogen). Fluorescently labeled secondary antibodies IR800CW and IR680RD (LI-COR Biosciences) were used at 1:5,000. Images of blots were obtained using Image Studio software (version 3.1; LI-COR Biosciences).

Cka double-stranded RNA

Double-stranded RNA against the 3′ UTR of *Cka* was prepared using PCR products as a template. Double-stranded RNA was prepared using the MEGASCRIPT T7 transcription kit (Thermo Fisher Scientific). Primers used were forward, 5′-TAATACGACTCACTATAGGGAGAAAGAGGCGAGACGAGACGAGA-3′, and reverse, 5′-TAATACGACTCACTATAGGGAGATTATTATTGTATGCATATAATTG-3′.

GeneSwitch neuronal depletion of CKA

The *elav-Switch.O* line was crossed to *UAS-CkaRNAi-B C911, UAS-CkaRNAi-B, UAS-CkaRNAi-B; UAS-BFP-Cka*, or *UAS-CkaRNAi-B; UAS-BFP-Cka*$^{\Delta PP2A}$. 200 µl of 0.6-mg/ml mifepristone (RU-486; Sigma-Aldrich) dissolved in 100% EtOH or 200 µl of 100% EtOH was mixed with 6 ml of standard cornmeal agar food for a final concentration of 20 µg/ml. Eggs were collected on juice plates, and 50 early third instar larvae (72 h after egg laying) were put into each vial. 100 larvae for each genotype were collected for each day of the experiment, which was performed over 3 d.

Online supplemental material

Fig. S1 compares the number of GFP-positive Atg8a puncta in terminal boutons for control animals versus animals depleted of a V-ATPase subunit, *Cka* transcripts and the predicted protein isoform mobilities, and immunoblots showing the levels of CKA protein in neurons versus glia. Fig. S2 shows plots for the number of autophagosomes per axon pair in control larvae by comparison to autophagosomes present in larval axons after depletion of CKA or dynein, the transport dynamics of autophagosomes in *syx17*^{LL} heterozygous and homozygous larvae, and

the anterograde flux of autophagosomes in control animals versus animals that were depleted of CKA or dynein. Fig. S3 displays immunoblots characterizing the capacity of Flag-CKA to coimmunoprecipitate with GFP-CKA, GFP-CKA^{mutLIR2}, or GFP-CKA$^{\Delta PP2A}$; immunoblots characterizing the capacity of MBP-Atg8 to bind and immunoprecipitate GFP-CKA, but not GFP-CKA^{mutLIR2}; a table documenting the mean numbers of motile DCVs present in control larvae and larvae depleted of CKA, Mob4, Strip, or dynein; and images of DCVs in axonal jams of larval axons in which CKA or dynein was depleted by RNAi. Fig. S4 includes a table of the mean numbers of motile mitochondria in control and experimental larvae depleted of dynein (dhc64c), CKA, Mob4, and Strip; immunoblots reporting the reduced ability of the mutant GFP-CKA$^{\Delta PP2A}$ to immunoprecipitate with Flag-Pp2A-29B by comparison to GFP-CKA and GFP-CKA^{mutLIR2} as well as the protein levels of BFP-CKA and BFP-CKA$^{\Delta PP2A}$ in larval brain lysates; and a table of the mean numbers of motile DCVs for CKA depletion and CKA rescue experiments. Video 1 compares uninduced (vehicle control) *Drosophila* with *Drosophila* treated with 20 µg/ml RU-486 as early third instar larvae to induce *Cka* depletion in neurons. Video 2 shows a closeup of adult *Drosophila* treated with 20 µg/ml RU-486 as early third instar larvae to induce *Cka* depletion in neurons. Video 3 shows a sequence-specific RNAi off-target control for *Cka* temporally expressed in neurons. Video 4 shows temporal *Cka* depletion and rescue with a *BFP-Cka* fusion protein in neurons. Video 5 shows temporal *Cka* depletion and rescue with a *BFP-Cka$^{\Delta PP2A}$* fusion protein in neurons. Video 6 shows a closeup of adult *Drosophila* treated with 20 µg/ml RU-486 as early third instar larvae to temporal *Cka* depletion and rescue with a *BFP-Cka$^{\Delta PP2A}$* fusion protein in neurons. Table S1 lists the genotypes used to evaluate the data for each of the experiments.

Acknowledgments

We thank members of the Hays and Neufeld laboratories for helpful feedback on this work. We thank Annamarie Allen for technical assistance. We are grateful to Wei Du and Takahiro Chihara for providing antibodies, Steven Hou for providing the *Cka^{2}* allele and *Cka* clone, Yunyun Jin and Lei Zhang for providing the *UAS-Flag-hpo* and *UAS-Flag-hpo^{T195E}* lines, and Richard Fehon for the *GFP-yki* construct. We thank Thomas Pengo for assistance with statistical analyses. We thank Sean Conner, Mary Porter, Adam Avery, Guillermo Marqués, Min-Gang Li, and Madeline Serr for critical reading of the manuscript. A portion of this work was done at the University of Minnesota University Imaging Centers.

This work was funded by the American Heart Association postdoctoral grant 15POST22790015 to A.L. Neisch, the National Institutes of Health grant 2R01GM062509 to T.P. Neufeld, and the National Institutes of Health grant 5R01GM044757 to T.S. Hays.

The authors declare no competing financial interests.

Submitted: 17 June 2016
Revised: 9 November 2016
Accepted: 27 December 2016

References

Aberle, H., A.P. Haghighi, R.D. Fetter, B.D. McCabe, T.R. Magalhães, and C.S. Goodman. 2002. *wishful thinking* encodes a BMP type II receptor that regulates synaptic growth in *Drosophila*. *Neuron.* 33:545–558. http://dx.doi.org/10.1016/S0896-6273(02)00589-5

Andreazza, S., S. Bouleau, B. Martin, A. Lamouroux, P. Ponien, C. Papin, E. Chélot, E. Jacquet, and F. Rouyer. 2015. Daytime CLOCK dephosphorylation is controlled by STRIPAK complexes in *Drosophila*. *Cell Reports.* 11:1266–1279. http://dx.doi.org/10.1016/j.celrep.2015.04.033

Berger, R.L. 1996a. More powerful tests from confidence interval p values. *Am. Stat.* 50:314–318. http://dx.doi.org/10.1080/00031305.1996.10473559

Berger, R.L.1996b. Exact unconditional homogeneity/independence tests for 2X2 tables. NC State University. http://www4.stat.ncsu.edu/~boos/exact/

Bose, A., A.T. Majot, and A.P. Bidwai. 2014. The Ser/Thr phosphatase PP2A regulatory subunit *widerborst* inhibits notch signaling. *PLoS One.* 9. http://dx.doi.org/10.1371/journal.pone.0101884

Bowman, A.B., A. Kamal, B.W. Ritchings, A.V. Philp, M. McGrail, J.G. Gindhart, and L.S. Goldstein. 2000. Kinesin-dependent axonal transport is mediated by the sunday driver (SYD) protein. *Cell.* 103:583–594. http://dx.doi.org/10.1016/S0092-8674(00)00162-8

Castets, F., T. Rakitina, S. Gaillard, A. Moqrich, M.G. Mattei, and A. Monneron. 2000. Zinedin, SG2NA, and striatin are calmodulin-binding, WD repeat proteins principally expressed in the brain. *J. Biol. Chem.* 275:19970–19977. http://dx.doi.org/10.1074/jbc.M909782199

Chang, Y.Y., and T.P. Neufeld. 2009. An Atg1/Atg13 complex with multiple roles in TOR-mediated autophagy regulation. *Mol. Biol. Cell.* 20:2004–2014. http://dx.doi.org/10.1091/mbc.E08-12-1250

Chen, C., Z. Shi, W. Zhang, M. Chen, F. He, Z. Zhang, Y. Wang, M. Feng, W. Wang, Y. Zhao, et al. 2014. Striatins contain a noncanonical coiled coil that binds protein phosphatase 2A A subunit to form a 2:2 heterotetrameric core of striatin-interacting phosphatase and kinase (STRIPAK) complex. *J. Biol. Chem.* 289:9651–9661. http://dx.doi.org/10.1074/jbc.M113.529297

Chen, H.W., M.J. Marinissen, S.W. Oh, X. Chen, M. Melnick, N. Perrimon, J.S. Gutkind, and S.X. Hou. 2002. CKA, a novel multidomain protein, regulates the JUN N-terminal kinase signal transduction pathway in *Drosophila*. *Mol. Cell. Biol.* 22:1792–1803. http://dx.doi.org/10.1128/MCB.22.6.1792-1803.2002

Cheng, X.T., B. Zhou, M.Y. Lin, Q. Cai, and Z.H. Sheng. 2015. Axonal autophagosomes recruit dynein for retrograde transport through fusion with late endosomes. *J. Cell Biol.* 209:377–386. http://dx.doi.org/10.1083/jcb.201412046

Couzens, A.L., J.D. Knight, M.J. Kean, G. Teo, A. Weiss, W.H. Dunham, Z.Y. Lin, R.D. Bagshaw, F. Sicheri, T. Pawson, et al. 2013. Protein interaction network of the mammalian Hippo pathway reveals mechanisms of kinase-phosphatase interactions. *Sci. Signal.* 6. http://dx.doi.org/10.1126/scisignal.2004712

Evans, D.R., T. Myles, J. Hofsteenge, and B.A. Hemmings. 1999. Functional expression of human PP2Ac in yeast permits the identification of novel C-terminal and dominant-negative mutant forms. *J. Biol. Chem.* 274:24038–24046. http://dx.doi.org/10.1074/jbc.274.34.24038

Fu, M.M., and E.L. Holzbaur. 2014. Integrated regulation of motor-driven organelle transport by scaffolding proteins. *Trends Cell Biol.* 24:564–574. http://dx.doi.org/10.1016/j.tcb.2014.05.002

Fu, M.M., J.J. Nirschl, and E.L. Holzbaur. 2014. LC3 binding to the scaffolding protein JIP1 regulates processive dynein-driven transport of autophagosomes. *Dev. Cell.* 29:577–590. http://dx.doi.org/10.1016/j.devcel.2014.04.015

Gao, F.J., S. Hebbar, X.A. Gao, M. Alexander, J.P. Pandey, M.D. Walla, W.E. Cotham, S.J. King, and D.S. Smith. 2015. GSK-3β phosphorylation of cytoplasmic dynein reduces Ndel1 binding to intermediate chains and alters dynein motility. *Traffic.* 16:941–961. http://dx.doi.org/10.1111/tra.12304

Gong, C.X., T.J. Singh, I. Grundke-Iqbal, and K. Iqbal. 1993. Phosphoprotein phosphatase activities in Alzheimer disease brain. *J. Neurochem.* 61:921–927. http://dx.doi.org/10.1111/j.1471-4159.1993.tb03603.x

Gordon, J., J. Hwang, K.J. Carrier, C.A. Jones, Q.L. Kern, C.S. Moreno, R.H. Karas, and D.C. Pallas. 2011. Protein phosphatase 2a (PP2A) binds within the oligomerization domain of striatin and regulates the phosphorylation and activation of the mammalian Ste20-like kinase Mst3. *BMC Biochem.* 12. http://dx.doi.org/10.1186/1471-2091-12-54

Goudreault, M., L.M. D'Ambrosio, M.J. Kean, M.J. Mullin, B.G. Larsen, A. Sanchez, S. Chaudhry, G.I. Chen, F. Sicheri, A.I. Nesvizhskii, et al. 2009. A PP2A phosphatase high density interaction network identifies a novel striatin-interacting phosphatase and kinase complex linked to the cerebral cavernous malformation 3 (CCM3) protein. *Mol. Cell. Proteomics.* 8:157–171. http://dx.doi.org/10.1074/mcp.M800266-MCP200

Gunawardena, S., L.S. Her, R.G. Brusch, R.A. Laymon, I.R. Niesman, B. Gordesky-Gold, L. Sintasath, N.M. Bonini, and L.S. Goldstein. 2003. Disruption of axonal transport by loss of huntingtin or expression of pathogenic polyQ proteins in *Drosophila*. *Neuron.* 40:25–40. http://dx.doi.org/10.1016/S0896-6273(03)00594-4

Hannus, M., F. Feiguin, C.P. Heisenberg, and S. Eaton. 2002. Planar cell polarization requires Widerborst, a B′ regulatory subunit of protein phosphatase 2A. *Development.* 129:3493–3503.

Hegedűs, K., S. Takáts, A.L. Kovács, and G. Juhász. 2013. Evolutionarily conserved role and physiological relevance of a STX17/Syx17 (syntaxin 17)-containing SNARE complex in autophagosome fusion with endosomes and lysosomes. *Autophagy.* 9:1642–1646. http://dx.doi.org/10.4161/auto.25684

Horiuchi, D., R.V. Barkus, A.D. Pilling, A. Gassman, and W.M. Saxton. 2005. APLIP1, a kinesin binding JIP-1/JNK scaffold protein, influences the axonal transport of both vesicles and mitochondria in *Drosophila*. *Curr. Biol.* 15:2137–2141. http://dx.doi.org/10.1016/j.cub.2005.10.047

Horiuchi, D., C.A. Collins, P. Bhat, R.V. Barkus, A. Diantonio, and W.M. Saxton. 2007. Control of a kinesin-cargo linkage mechanism by JNK pathway kinases. *Curr. Biol.* 17:1313–1317. http://dx.doi.org/10.1016/j.cub.2007.06.062

Hurd, D.D., and W.M. Saxton. 1996. Kinesin mutations cause motor neuron disease phenotypes by disrupting fast axonal transport in Drosophila. *Genetics.* 144:1075–1085.

Hwang, J., and D.C. Pallas. 2014. STRIPAK complexes: structure, biological function, and involvement in human diseases. *Int. J. Biochem. Cell Biol.* 47:118–148. http://dx.doi.org/10.1016/j.biocel.2013.11.021

Hyodo, T., S. Ito, H. Hasegawa, E. Asano, M. Maeda, T. Urano, M. Takahashi, M. Hamaguchi, and T. Senga. 2012. Misshapen-like kinase 1 (MINK1) is a novel component of striatin-interacting phosphatase and kinase (STRIPAK) and is required for the completion of cytokinesis. *J. Biol. Chem.* 287:25019–25029. http://dx.doi.org/10.1074/jbc.M112.372342

Ikenaka, K., K. Kawai, M. Katsuno, Z. Huang, Y.M. Jiang, Y. Iguchi, K. Kobayashi, T. Kimata, M. Waza, F. Tanaka, et al. 2013. *dnc-1/dynactin 1* knockdown disrupts transport of autophagosomes and induces motor neuron degeneration. *PLoS One.* 8. http://dx.doi.org/10.1371/journal.pone.0054511

Kalvari, I., S. Tsompanis, N.C. Mulakkal, R. Osgood, T. Johansen, I.P. Nezis, and V.J. Promponas. 2014. iLIR: A web resource for prediction of Atg8-family interacting proteins. *Autophagy.* 10:913–925. http://dx.doi.org/10.4161/auto.28260

Kean, M.J., D.F. Ceccarelli, M. Goudreault, M. Sanches, S. Tate, B. Larsen, L.C. Gibson, W.B. Derry, I.C. Scott, L. Pelletier, et al. 2011. Structure-function analysis of core STRIPAK proteins: a signaling complex implicated in Golgi polarization. *J. Biol. Chem.* 286:25065–25075. http://dx.doi.org/10.1074/jbc.M110.214486

Kelkar, N., S. Gupta, M. Dickens, and R.J. Davis. 2000. Interaction of a mitogen-activated protein kinase signaling module with the neuronal protein JIP3. *Mol. Cell. Biol.* 20:1030–1043. http://dx.doi.org/10.1128/MCB.20.3.1030-1043.2000

Kimura, S., T. Noda, and T. Yoshimori. 2007. Dissection of the autophagosome maturation process by a novel reporter protein, tandem fluorescent-tagged LC3. *Autophagy.* 3:452–460. http://dx.doi.org/10.4161/auto.4451

Kimura, S., T. Noda, and T. Yoshimori. 2008. Dynein-dependent movement of autophagosomes mediates efficient encounters with lysosomes. *Cell Struct. Funct.* 33:109–122. http://dx.doi.org/10.1247/csf.08005

Klinman, E., and E.L. Holzbaur. 2015. Stress-induced CDK5 activation disrupts axonal transport via Lis1/Ndel1/dynein. *Cell Reports.* 12:462–473. http://dx.doi.org/10.1016/j.celrep.2015.06.032

Lant, B., B. Yu, M. Goudreault, D. Holmyard, J.D. Knight, P. Xu, L. Zhao, K. Chin, E. Wallace, M. Zhen, et al. 2015. CCM-3/STRIPAK promotes seamless tube extension through endocytic recycling. *Nat. Commun.* 6. http://dx.doi.org/10.1038/ncomms7449

Li, L., X. Tian, M. Zhu, D. Bulgari, M.A. Böhme, F. Goettfert, C. Wichmann, S.J. Sigrist, E.S. Levitan, and C. Wu. 2014. *Drosophila* Syd-1, liprin-α, and protein phosphatase 2A B′ subunit Wrd function in a linear pathway to prevent ectopic accumulation of synaptic materials in distal axons. *J. Neurosci.* 34:8474–8487. http://dx.doi.org/10.1523/JNEUROSCI.0409-14.2014

Liu, B., Y. Zheng, F. Yin, J. Yu, N. Silverman, and D. Pan. 2016. Toll receptor-mediated Hippo signaling controls innate immunity in *Drosophila*. *Cell.* 164:406–419. http://dx.doi.org/10.1016/j.cell.2015.12.029

Lloyd, T.E., J. Machamer, K. O'Hara, J.H. Kim, S.E. Collins, M.Y. Wong, B. Sahin, W. Imlach, Y. Yang, E.S. Levitan, et al. 2012. The $p150^{Glued}$ CAP-Gly domain regulates initiation of retrograde transport at synaptic termini. *Neuron.* 74:344–360. http://dx.doi.org/10.1016/j.neuron.2012.02.026

Lystad, A.H., Y. Ichimura, K. Takagi, Y. Yang, S. Pankiv, Y. Kanegae, S. Kageyama, M. Suzuki, I. Saito, T. Mizushima, et al. 2014. Structural determinants in GABARAP required for the selective binding and recruitment of ALFY to LC3B-positive structures. *EMBO Rep.* 15:557–565. http://dx.doi.org/10.1002/embr.201338003

Maday, S., K.E. Wallace, and E.L. Holzbaur. 2012. Autophagosomes initiate distally and mature during transport toward the cell soma in primary neurons. *J. Cell Biol.* 196:407–417. http://dx.doi.org/10.1083/jcb.201106120

Martin, M., S.J. Iyadurai, A. Gassman, J.G. Gindhart Jr., T.S. Hays, and W.M. Saxton. 1999. Cytoplasmic dynein, the dynactin complex, and kinesin are interdependent and essential for fast axonal transport. *Mol. Biol. Cell.* 10:3717–3728. http://dx.doi.org/10.1091/mbc.10.11.3717

Matsuda, S., T. Yasukawa, Y. Homma, Y. Ito, T. Niikura, T. Hiraki, S. Hirai, S. Ohno, Y. Kita, M. Kawasumi, et al. 2001. c-Jun N-terminal kinase (JNK)-interacting protein-1b/islet-brain-1 scaffolds Alzheimer's amyloid precursor protein with JNK. *J. Neurosci.* 21:6597–6607.

Mauvezin, C., C. Ayala, C.R. Braden, J. Kim, and T.P. Neufeld. 2014. Assays to monitor autophagy in *Drosophila*. *Methods.* 68:134–139. http://dx.doi.org/10.1016/j.ymeth.2014.03.014

Mauvezin, C., P. Nagy, G. Juhász, and T.P. Neufeld. 2015. Autophagosome-lysosome fusion is independent of V-ATPase-mediated acidification. *Nat. Commun.* 6. http://dx.doi.org/10.1038/ncomms8007

Mauvezin, C., A.L. Neisch, C.I. Ayala, J. Kim, A. Beltrame, C.R. Braden, M.K. Gardner, T.S. Hays, and T.P. Neufeld. 2016. Coordination of autophagosome-lysosome fusion and transport by a Klp98A-Rab14 complex in *Drosophila*. *J. Cell Sci.* 129:971–982. http://dx.doi.org/10.1242/jcs.175224

McEwan, D.G., D. Popovic, A. Gubas, S. Terawaki, H. Suzuki, D. Stadel, F.P. Coxon, D. Miranda de Stegmann, S. Bhogaraju, K. Maddi, et al. 2015. PLEKHM1 regulates autophagosome-lysosome fusion through HOPS complex and LC3/GABARAP proteins. *Mol. Cell.* 57:39–54. http://dx.doi.org/10.1016/j.molcel.2014.11.006

McGrail, M., and T.S. Hays. 1997. The microtubule motor cytoplasmic dynein is required for spindle orientation during germline cell divisions and oocyte differentiation in Drosophila. *Development.* 124:2409–2419.

Meléndez, A., and T.P. Neufeld. 2008. The cell biology of autophagy in metazoans: a developing story. *Development.* 135:2347–2360. http://dx.doi.org/10.1242/dev.016105

Mitchell, D.J., K.R. Blasier, E.D. Jeffery, M.W. Ross, A.K. Pullikuth, D. Suo, J. Park, W.R. Smiley, K.W. Lo, J. Shabanowitz, et al. 2012. Trk activation of the ERK1/2 kinase pathway stimulates intermediate chain phosphorylation and recruits cytoplasmic dynein to signaling endosomes for retrograde axonal transport. *J. Neurosci.* 32:15495–15510. http://dx.doi.org/10.1523/JNEUROSCI.5599-11.2012

Mizushima, N., T. Yoshimori, and B. Levine. 2010. Methods in mammalian autophagy research. *Cell.* 140:313–326. http://dx.doi.org/10.1016/j.cell.2010.01.028

Mohr, S.E., J.A. Smith, C.E. Shamu, R.A. Neumüller, and N. Perrimon. 2014. RNAi screening comes of age: improved techniques and complementary approaches. *Nat. Rev. Mol. Cell Biol.* 15:591–600. http://dx.doi.org/10.1038/nrm3860

Moreno, C.S., W.S. Lane, and D.C. Pallas. 2001. A mammalian homolog of yeast MOB1 is both a member and a putative substrate of striatin family-protein phosphatase 2A complexes. *J. Biol. Chem.* 276:24253–24260. http://dx.doi.org/10.1074/jbc.M102398200

Moughamian, A.J., and E.L. Holzbaur. 2012. Dynactin is required for transport initiation from the distal axon. *Neuron.* 74:331–343. http://dx.doi.org/10.1016/j.neuron.2012.02.025

Neisch, A.L., A.W. Avery, J.B. Machamer, M.G. Li, and T.S. Hays. 2016. Methods to identify and analyze gene products involved in neuronal intracellular transport using *Drosophila*. *Methods Cell Biol.* 131:277–309. http://dx.doi.org/10.1016/bs.mcb.2015.06.015

Nirschl, J.J., M.M. Magiera, J.E. Lazarus, C. Janke, and E.L. Holzbaur. 2016. α-Tubulin tyrosination and CLIP-170 phosphorylation regulate the initiation of dynein-driven transport in neurons. *Cell Reports.* 14:2637–2652. http://dx.doi.org/10.1016/j.celrep.2016.02.046

Nixon, R.A., J. Wegiel, A. Kumar, W.H. Yu, C. Peterhoff, A. Cataldo, and A.M. Cuervo. 2005. Extensive involvement of autophagy in Alzheimer disease: an immuno-electron microscopy study. *J. Neuropathol. Exp. Neurol.* 64:113–122. http://dx.doi.org/10.1093/jnen/64.2.113

Osterwalder, T., K.S. Yoon, B.H. White, and H. Keshishian. 2001. A conditional tissue-specific transgene expression system using inducible GAL4. *Proc. Natl. Acad. Sci. USA.* 98:12596–12601. http://dx.doi.org/10.1073/pnas.221303298

Ostlund, G., T. Schmitt, K. Forslund, T. Köstler, D.N. Messina, S. Roopra, O. Frings, and E.L. Sonnhammer. 2010. InParanoid 7: new algorithms and tools for eukaryotic orthology analysis. *Nucleic Acids Res.* 38:D196–D203. http://dx.doi.org/10.1093/nar/gkp931

Pandey, J.P., and D.S. Smith. 2011. A Cdk5-dependent switch regulates Lis1/Ndel1/dynein-driven organelle transport in adult axons. *J. Neurosci.* 31:17207–17219. http://dx.doi.org/10.1523/JNEUROSCI.4108-11.2011

Pankiv, S., T.H. Clausen, T. Lamark, A. Brech, J.A. Bruun, H. Outzen, A. Øvervatn, G. Bjørkøy, and T. Johansen. 2007. p62/SQSTM1 binds directly to Atg8/LC3 to facilitate degradation of ubiquitinated protein aggregates by autophagy. *J. Biol. Chem.* 282:24131–24145. http://dx.doi.org/10.1074/jbc.M702824200

Pankiv, S., E.A. Alemu, A. Brech, J.A. Bruun, T. Lamark, A. Overvatn, G. Bjørkøy, and T. Johansen. 2010. FYCO1 is a Rab7 effector that binds to LC3 and PI3P to mediate microtubule plus end-directed vesicle transport. *J. Cell Biol.* 188:253–269. http://dx.doi.org/10.1083/jcb.200907015

Pilling, A.D., D. Horiuchi, C.M. Lively, and W.M. Saxton. 2006. Kinesin-1 and dynein are the primary motors for fast transport of mitochondria in *Drosophila* motor axons. *Mol. Biol. Cell.* 17:2057–2068. http://dx.doi.org/10.1091/mbc.E05-06-0526

Rao, S., C. Lang, E.S. Levitan, and D.L. Deitcher. 2001. Visualization of neuropeptide expression, transport, and exocytosis in *Drosophila melanogaster*. *J. Neurobiol.* 49:159–172. http://dx.doi.org/10.1002/neu.1072

Ravikumar, B., A. Acevedo-Arozena, S. Imarisio, Z. Berger, C. Vacher, C.J. O'Kane, S.D. Brown, and D.C. Rubinsztein. 2005. Dynein mutations impair autophagic clearance of aggregate-prone proteins. *Nat. Genet.* 37:771–776. http://dx.doi.org/10.1038/ng1591

Ribeiro, P.S., F. Josué, A. Wepf, M.C. Wehr, O. Rinner, G. Kelly, N. Tapon, and M. Gstaiger. 2010. Combined functional genomic and proteomic approaches identify a PP2A complex as a negative regulator of Hippo signaling. *Mol. Cell.* 39:521–534. http://dx.doi.org/10.1016/j.molcel.2010.08.002

Rudrabhatla, P. 2014. Regulation of neuronal cytoskeletal protein phosphorylation in neurodegenerative diseases. *J. Alzheimers Dis.* 41:671–684. http://dx.doi.org/10.3233/JAD-130794

Sakuma, C., T. Kawauchi, S. Haraguchi, M. Shikanai, Y. Yamaguchi, V.I. Gelfand, L. Luo, M. Miura, and T. Chihara. 2014. *Drosophila* Strip serves as a platform for early endosome organization during axon elongation. *Nat. Commun.* 5. http://dx.doi.org/10.1038/ncomms6180

Sakuma, C., M. Okumura, T. Umehara, M. Miura, and T. Chihara. 2015. A STR IPAK component Strip regulates neuronal morphogenesis by affecting microtubule stability. *Sci. Rep.* 5. http://dx.doi.org/10.1038/srep17769

Scheinfeld, M.H., R. Roncarati, P. Vito, P.A. Lopez, M. Abdallah, and L. D'Adamio. 2002. Jun NH2-terminal kinase (JNK) interacting protein 1 (JIP1) binds the cytoplasmic domain of the Alzheimer's β-amyloid precursor protein (APP). *J. Biol. Chem.* 277:3767–3775. http://dx.doi.org/10.1074/jbc.M108357200

Schlager, M.A., and C.C. Hoogenraad. 2009. Basic mechanisms for recognition and transport of synaptic cargos. *Mol. Brain.* 2. http://dx.doi.org/10.1186/1756-6606-2-25

Schulte, J., K.J. Sepp, R.A. Jorquera, C. Wu, Y. Song, P. Hong, and J.T. Littleton. 2010. DMob4/Phocein regulates synapse formation, axonal transport, and microtubule organization. *J. Neurosci.* 30:5189–5203. http://dx.doi.org/10.1523/JNEUROSCI.5823-09.2010

Scott, R.C., G. Juhász, and T.P. Neufeld. 2007. Direct induction of autophagy by Atg1 inhibits cell growth and induces apoptotic cell death. *Curr. Biol.* 17:1–11. http://dx.doi.org/10.1016/j.cub.2006.10.053

Shibutani, S.T., and T. Yoshimori. 2014. A current perspective of autophagosome biogenesis. *Cell Res.* 24:58–68. http://dx.doi.org/10.1038/cr.2013.159

Song, Y., M. Eng, and A.S. Ghabrial. 2013. Focal defects in single-celled tubes mutant for *Cerebral cavernous malformation 3*, *GCKIII*, or *NSF2*. *Dev. Cell.* 25:507–519. http://dx.doi.org/10.1016/j.devcel.2013.05.002

Sontag, J.M., and E. Sontag. 2014. Protein phosphatase 2A dysfunction in Alzheimer's disease. *Front. Mol. Neurosci.* 7. http://dx.doi.org/10.3389/fnmol.2014.00016

Sun, D., and L. Buttitta. 2015. Protein phosphatase 2A promotes the transition to G0 during terminal differentiation in *Drosophila*. *Development.* 142:3033–3045. http://dx.doi.org/10.1242/dev.120824

Swarup, S., T. Pradhan-Sundd, and E.M. Verheyen. 2015. Genome-wide identification of phospho-regulators of Wnt signaling in *Drosophila*. *Development.* 142:1502–1515. http://dx.doi.org/10.1242/dev.116715

Takáts, S., P. Nagy, Á. Varga, K. Pircs, M. Kárpáti, K. Varga, A.L. Kovács, K. Hegedűs, and G. Juhász. 2013. Autophagosomal Syntaxin17-dependent lysosomal degradation maintains neuronal function in *Drosophila*. *J. Cell Biol.* 201:531–539. http://dx.doi.org/10.1083/jcb.201211160

Vaughan, P.S., J.D. Leszyk, and K.T. Vaughan. 2001. Cytoplasmic dynein intermediate chain phosphorylation regulates binding to dynactin. *J. Biol. Chem.* 276:26171–26179. http://dx.doi.org/10.1074/jbc.M102649200

Viquez, N.M., C.R. Li, Y.P. Wairkar, and A. DiAntonio. 2006. The B′ protein phosphatase 2A regulatory subunit *well-rounded* regulates synaptic growth and cytoskeletal stability at the *Drosophila* neuromuscular junction. *J. Neurosci.* 26:9293–9303. http://dx.doi.org/10.1523/JNEUROSCI.1740-06.2006

Viquez, N.M., P. Füger, V. Valakh, R.W. Daniels, T.M. Rasse, and A. DiAntonio. 2009. PP2A and GSK-3β act antagonistically to regulate active zone development. *J. Neurosci.* 29:11484–11494. http://dx.doi.org/10.1523/JNEUROSCI.5584-08.2009

Wang, C., K.C. Chang, G. Somers, D. Virshup, B.T. Ang, C. Tang, F. Yu, and H. Wang. 2009. Protein phosphatase 2A regulates self-renewal of *Drosophila* neural stem cells. *Development.* 136:2287–2296. http://dx.doi.org/10.1242/dev.035758

Wang, P., M. Larouche, K. Normandin, D. Kachaner, H. Mehsen, G. Emery, and V. Archambault. 2016. Spatial regulation of greatwall by Cdk1 and PP2A-Tws in the cell cycle. *Cell Cycle.* 15:528–539. http://dx.doi.org/10.1080/15384101.2015.1127476

Weaver, C., C. Leidel, L. Szpankowski, N.M. Farley, G.T. Shubeita, and L.S. Goldstein. 2013. Endogenous GSK-3/shaggy regulates bidirectional axonal transport of the amyloid precursor protein. *Traffic.* 14:295–308. http://dx.doi.org/10.1111/tra.12037

Willoughby, E.A., G.R. Perkins, M.K. Collins, and A.J. Whitmarsh. 2003. The JNK-interacting protein-1 scaffold protein targets MAPK phosphatase-7 to dephosphorylate JNK. *J. Biol. Chem.* 278:10731–10736. http://dx.doi.org/10.1074/jbc.M207324200

Wong, Y.C., and E.L. Holzbaur. 2014a. Optineurin is an autophagy receptor for damaged mitochondria in parkin-mediated mitophagy that is disrupted by an ALS-linked mutation. *Proc. Natl. Acad. Sci. USA.* 111:E4439–E4448. http://dx.doi.org/10.1073/pnas.1405752111

Wong, Y.C., and E.L. Holzbaur. 2014b. The regulation of autophagosome dynamics by huntingtin and HAP1 is disrupted by expression of mutant huntingtin, leading to defective cargo degradation. *J. Neurosci.* 34:1293–1305. http://dx.doi.org/10.1523/JNEUROSCI.1870-13.2014

Wu, S., J. Huang, J. Dong, and D. Pan. 2003. *hippo* encodes a Ste-20 family protein kinase that restricts cell proliferation and promotes apoptosis in conjunction with *salvador* and *warts*. *Cell.* 114:445–456. http://dx.doi.org/10.1016/S0092-8674(03)00549-X

Xiong, X., X. Wang, R. Ewanek, P. Bhat, A. Diantonio, and C.A. Collins. 2010. Protein turnover of the Wallenda/DLK kinase regulates a retrograde response to axonal injury. *J. Cell Biol.* 191:211–223. http://dx.doi.org/10.1083/jcb.201006039

Xu, M., X.X. Li, J. Xiong, M. Xia, E. Gulbins, Y. Zhang, and P.L. Li. 2013. Regulation of autophagic flux by dynein-mediated autophagosomes trafficking in mouse coronary arterial myocytes. *Biochim. Biophys. Acta.* 1833:3228–3236. http://dx.doi.org/10.1016/j.bbamcr.2013.09.015

Yasuda, J., A.J. Whitmarsh, J. Cavanagh, M. Sharma, and R.J. Davis. 1999. The JIP group of mitogen-activated protein kinase scaffold proteins. *Mol. Cell. Biol.* 19:7245–7254. http://dx.doi.org/10.1128/MCB.19.10.7245